Stereoselective Synthesis of a 4-□-Glucoside of Valienamine, Inhibition, and X-Ray Structural Studies Involving a Bacterial Glycoside Hydrolase-Like Enzyme of The GH13 Family

Si Anshupriya
University of Toledo
Thilina D. Jayasinghe
University of Nebraska Medical Center
Radhika Thanvi
University of Toledo
Donald R. Ronning
University of Nebraska Medical Center
Steven J. Sucheck (steve.sucheck@utoledo.edu)
University of Toledo

Research Article

Keywords: Glycoside hydrolases (GH), cyclohexene fragment, aminocarbasugar-based GH13-inhibitors, hydrolytic enzymes

Posted Date: March 22nd, 2021

DOI: https://doi.org/10.21203/rs.3.rs-322389/v1

Abstract

Glycoside hydrolases (GH) are a large family of hydrolytic enzymes found in all domains of life. As such, they control a plethora of normal and pathogenic biological functions. Thus, understanding selective inhibition of GH enzymes at the atomic level can lead to the identification of new classes of therapeutics. In these studies, we identified a 4-□-glucoside of valienamine (**8**) as an inhibitor (IC_{50} of 484 ± 51 μM) of *Streptomyces coelicolor* (*Sco*) GlgE1-V279S which belongs to the GH13 Carbohydrate Active EnZyme (CAZy) family. The synthetic route to **8** and a closely related 4-□-glucoside of validamine (**7**) was achieved starting from readily available D-maltose. A key step in the synthesis was a chelation-controlled addition of vinylmagnesium bromide to a maltose-derived enone intermediate. X-ray structures of both **7** and **8** in complex with *Sco* GlgE1-V279S were solved to resolutions of 1.75 and 1.78 Å, respectively. Structural analysis revealed the valienamine derivative **8** binds the enzyme in an E_2 conformation for the cyclohexene fragment. Also, the cyclohexene fragment shows a new hydrogen-bonding contact from the pseudo-diaxial C(3)-OH to the catalytic nucleophile Asp 394 at the enzyme active site. Asp 394, in fact, forms a bidentate interaction with both the C(3)-OH and C(7)-OH of the inhibitor. In contrast, compound **7** disrupts the catalytic sidechain interaction network of *Sco* GlgE1-V279S via steric interactions resulting in a conformation change in Asp 394. These findings will have implications for the design other aminocarbasugar-based GH13-inhibitors and will be useful for identifying more potent and selective inhibitors.

Introduction

Glycoside hydrolase (GH) enzymes are hydrolases involved in a large array of biological phenomena.[1-3] Inhibiting the GH activity alters the glycosylation or catabolism of glycans, making the GH inhibitors highly potent drugs.[4-7] An important class of GH inhibitors in glycobiology are the carbasugars, wherein the endocyclic ring oxygen is replaced by a methylene group or an sp^2 hybridized carbon.[8,9] Some of these pseudosaccharides may mimic the transition state (TS) of the catalyzed reaction while others may mimic the Michaelis complex.[4] The exact nature of GH inhibition by carbasugars remains complex as to whether they are actual TS inhibitors or merely tight binders.[10-13] 1-Aminocarbasugars are thought to mimic charge development in the TS by incorporating a basic nitrogen atom in place of C(1)-O.[14] One example of this compound class is Acarbose (**1**), an inhibitor of the GH13 enzyme human pancreatic α-amylase and a treatment for type-II diabetes mellitus (T2D), Figure 1,[15,16] while aminocarbasugars related to validamine (**2a**) and valienamine (**6**)[17,18] show inhibitory activity against α-GHs such as α-amylase, rice α-glucosidase and yeast α-glucosidase.[19,20] IC_{50} values for compounds **2** – **6** against α-amylase are in the range of 10^{-2} mol/L and against yeast α-glucosidase is between 10^{-5} – 10^{-4} mol/L.[19] Voglibose (**5**), a derivative of **2a**, has also found use as an α-glucosidase inhibitor and treatment for T2D.[20] The inhibitory activities of **1** and related compounds has been commonly ascribed to the ability to mimic a glucopyranosyl half-chair conformation intermediate of glycosidase catalysis[12,15,21] and form favorable coulombic interactions.[22] For valienamine-base carbasugars, an initial Michaelis complex in the $^2H_3$

conformation is postulated.[23] However, there is limited information on the conformational itinerary of natural GH13 substrates.[24,25] Based on these reports, we proposed the 4-α-glucoside of validamine (**7**) and 4-α-glucoside of valienamine (**8**) would be potential inhibitors of α-GHs that can accommodate an α-configured -2 site sugar, for example, *Sco* GlgE1-V279S, Figure 1.

The GlgE homologs of Streptomyces and Mycobacteria catalyze the conversion of maltose-1-phosphate (M1P) to linear α-(1→4) glucans which play an important role in the bacterial cell wall formation, Figure 2A.[26] *Mtb* GlgE is a genetically validated anti-TB target as the absence of *Mtb* GlgE leads to cytosolic accumulation of toxic levels of M1P by a self-amplifying feedback response leading to cell death.[26] Previously, we have shown that hydroxypyrrolidines modified with an α-configured -2 site sugar can inhibit *Mtb* GlgE (K_i = 237 ± 27 μM) as well *Sco* GlgE1-V279S (K_i = 102 ± 7 μM), a closely related homolog from *Streptomyces coelicolor* (*Sco*) GlgE1 that has been mutated to be 100 % identical to the M1P binding site of *Mtb* GlgE, and affords much higher quality X-ray diffraction data.[27]

Keeping in mind that *Sco* GlgE1 is an α-retaining glycoside hydrolase-like phosphorylase that uses a two-step substitution mechanism involving participation by an enzymatic nucleophile and general acid,[28,29] we proposed 1-aminocarbasugar **7** or **8** could form either Michaelis-like or TS-like contacts with *Sco* GlgE1-V279S and would form favorable coulombic interactions with the Glu 432 general acid, Figure 2B. In addition, it is appreciated that the TSs for GH are considered to have oxocarbenium-like character and it has been noted that $B_{2,5}$, $^{2,5}B$, $^{4}H_{3}$, and $^{3}H_{4}$ pyranose conformations should stabilize oxocarbenium character [30,31], Figure 2C. A putative pre-TS $^{3}S_{1}$ conformation is shown in equilibrium with the $^{3}H_{4}$-TS for later discussion. While compound **7** or **8** cannot completely mimic the possible TSs or the pre-TS conformations, compound **8** can exist in a $^{2}H_{3}$ conformation or $^{3}H_{2}$ conformation, Figure 2D. Also, higher energy conformations such as E_2 may be accessed depending on binding forces that could, and do (*vide infra*), develop in an enzyme-inhibitor complex. Consequently, our target carbasugars **7** and **8** were synthesized, evaluated for inhibition against *Sco* GlgE1-V279S, and their X-ray crystal structures solved in complex with *Sco* GlgE1-V279S to characterize the lowest energy conformations stabilized through interactions within the enzyme active site.

Previously, Tadashi et al. reported the enzymatic syntheses of α- and β-glucoside derivatives of validamine (**2a**) and valienamine (**6**) using maltose as a glucose donor in a glucosidase catalyzed transglycosylation.[17,18] The acceptors **2a** and **6** were obtained via microbial degradation of validamycin A by culturing soil bacteria *Pseudomonas denitrificans*[32] and *Flavobacterium saccharophilum*,[33] respectively, and isolating the products by ion-exchange chromatography. α- and β-glucosidases were extracted from *Rhodotorula lactosa*, purified by carboxymethyl (CM)-cellulose chromatography and used for catalyzing the α- and β-transglucosidations, respectively. 7-α-Isomaltoside and 4-α-glucoside (**7**) from **2a** and 7-α-glucoside, 7-α-isomaltoside, 4-α-isomaltoside and 4-α-glucoside (**8**) from **6** were some of the products obtained from these transglucosidation reactions. The inhibitory test results of these derivatives

against various α-glucosidases like rat intestinal maltase, sucrase, glucoamylase, isomaltase and trehalase suggested that **2a**, **6**, **7** and **8** are highly potent (IC_{50} = 10^{-5} to 10^{-2} M).[17,18]

However, relying on natural products and enzymatic methods to obtain **7** and **8** is very challenging due to the availability of biological sources, complex purifications, and complex spectroscopic characterization of closely related regioisomers. In order to overcome these difficulties, the development of an efficient synthetic strategy for the aminocarbasugars **7** and **8** was developed. In 1999, Kapferer et al. reported a practical synthetic route to the formation of valienamine (**6**) that involved a stereoselective addition of vinyl magnesium bromide to give separable dienes followed by a ring closing metathesis to give a cyclohexene adduct which could be transformed to the desired **6**.[34] In this work, we applied this method to the regiospecific synthesis of aminocarbasugars **7** and **8**. Scheme 1 illustrates the retrosynthetic route for the desired target inhibitors. Compounds **7** and **8** were then prepared in fourteen steps using commercially available D-(+)-maltose as the starting material.

Experimental Methods

General methods

All chemicals and solvents were purchased from Fisher Scientific, Acros Organics, Alfa Aesar or Sigma-Aldrich. Solvents were dried by through solvent purification system by passing through activated alumina and copper catalyst columns. All reactions were carried out at room temperature under a nitrogen atmosphere using a nitrogen balloon unless mentioned otherwise. Reactions were monitored by TLC (silica gel, f_{254}) under UV light or by charring (5% H_2SO_4-MeOH) and the purification was performed by column chromatography on silica gel (230-400 mesh) using the solvent system specified, solvents were used without purification for chromatography. ^{1}H NMR was recorded on Bruker Avance III 600 MHz spectrometer using $CDCl_3$ and D_2O as an internal reference. ^{13}C were recorded on Bruker Avance III 600 MHz spectrometer using $CDCl_3$ and D_2O as internal reference. High resolution mass spectrometry was recorded on TOF MS-ES+ instrument. Low resolution mass spectrometry was recorded on ESquire-LC-MS.

Metathesis procedure

A solution of dialkene in dichloromethane was degassed by passing nitrogen gas through it for 20 minutes. After that, 1st generation Grubb's catalyst (10 mol%) was added to the solution and the reaction was kept under nitrogen atmosphere using nitrogen balloon for 7 days or until the catalyst turned dark brown or black. Then, everything was evaporated under reduced pressure and purified using flash column chromatography on silica gel.

1,2,3,6,2' ,3' ,4' ,6'-octa-*O*-acetyl-D-maltose (21)[65]

D-(+)-Maltose monohydrate (2.00 g, 5.84 mmol) was suspended in dry pyridine (7.20 mL, 89.0 mmol) and acetic anhydride (6.28 mL, 66.8 mmol). A catalytic amount of 4-(dimethylamino)pyridine was added to

the solution. The solution was stirred at ambient temperature for 16 h. The reaction mixture was diluted with ethyl acetate and washed successively with 1 N HCl (20 mL) and saturated aq. $NaHCO_3$ (40 mL). The resulting organic phase was dried with anhydrous Na_2SO_4, filtered and the filtrate was concentrated under reduced pressure to give product **21**: yield 95% (3.50 g); silica gel TLC R_f = 0.5 (50% ethyl acetate : hexane). All the NMR values match with the reported data**.** [65]

4-methylphenyl 1-thio-β-D-maltopyranopyranoside (22)[66]

Peracetylated maltose **21** (3.45 g, 5.08 mmol) was dissolved in dichloromethane. 4-Methylthiophenol (1.26 g, 10.2 mmol) and boron trifluoride diethyl etherate (0.75 mL, 6.10 mmol) were added to the solution at 0 °C. The resulting solution was stirred at ambient temperature under nitrogen atmosphere. The reaction was monitored by TLC and appeared to be complete after 4 h. The reaction mixture was diluted with dichloromethane (20 mL) and successively washed with saturated aq. $NaHCO_3$ (25 mL), brine (25 mL), and water (15 mL). The resulting organic phase was dried (anhydrous Na_2SO_4), filtered and the filtrate was concentrated under reduced pressure. The product was dried overnight and deacetylated by dissolving in dry methanol followed by addition of a catalytic amount of sodium metal until the solution reached pH 9. The reaction was monitored for completion using TLC. The reaction was neutralized by adding Amberlite IRA-118H H^+ resin until the pH reached 7. Then, the resin was filtered away and the filtrate was concentrated under reduced pressure to afford the 4-methylthiophenyl maltoside **22**: yield 90% (3.10 g). All the NMR values match with the reported data.[66]

4-methylthiophenyl 2,3,6-Tri-*O*-benzyl-4-*O*-(2',3',4',6'-tetra-*O*-benzyl-α-D-glucopyranosyl)-β-D-glucopyranoside (23)[67]

A solution of **22** (2.95 g, 9.04 mmol) in dry *N,N*-dimethylformamide (50 mL) was cooled to 0 °C. The solution was treated drop-wise with a suspension of sodium hydride (60% dispersion in mineral oil) (4.55 g, 114.0 mmol) in dry *N,N*-dimethylformamide. Benzyl bromide (11.6 mL, 95.3 mmol) was added drop-wise over 15 min. and the solution stirred at room temperature for 16 h. The reaction was poured over ice and extracted with ethyl acetate (50 mL). The combined organic layers were washed with brine. The resulting organic phase was dried (anhydrous Na_2SO_4), filtered and the filtrate was concentrated under reduced pressure to obtain a product. The product was purified by silica gel flash column chromatography. The product fractions were combined, concentrated, and dried in vacuum to afford a yellow oily product **23**: yield 85% (2.50 g); silica gel TLC R_f = 0.61 (25% ethyl acetate : hexane). All the NMR values match with the reported data.[67]

2,3,6-Tri-*O*-benzyl-4-*O*-(2',3',4',6'-tetra-O-benzyl-α-D-glucopyranosyl)-α/β-D-glucopyranoside (24)[44]

N-bromosuccinimide (0.90 g, 5.08 mmol) was added to a solution of **6** (2.47 g, 2.45 mmol) in 9:1 acetone-water (50 mL) and stirred at room temperature for 45 min. The solvent was evaporated at room temperature until turbid. A solution of the residue in ethyl acetate (100 mL) was washed successively with saturated aqueous $NaHCO_3$, (3 X 50 mL) and water (3 X 50 mL). The solution was dried with

anhydrous Na_2SO_4 and evaporated. The product was purified by silica gel flash column chromatography. The product fractions were combined, concentrated, and dried in vacuum to afford a yellow oil **24**: yield 97% (2.40 g); silica gel TLC R_f = 0.19 (30% ethyl acetate : hexane). All the NMR values match with the reported data.[44]

3,4,7-Tri-*O*-benyl-5-*O*-(2',3',4',6'-tetra-*O*-benzyl-α-D-glucopyranosyl)-D-gluchept-1-enitol (25)[45]

n-Butyl lithium (2.22 M) in hexanes (5.3 mL, 12.0 mmol) was added drop-wise to a suspension of methyltriphenylphosphonium bromide (3.36 g, 9.44 mmol) in tetrahydrofuran (50 mL) at −20 °C. The solution was stirred at −20 °C for 15 min. and raised to ambient temperature over 1 h. The solution was cooled to −20 °C and compound **24** (2.30 g, 2.36 mmol) dissolved in 50 mL of tetrahydrofuran was added drop-wise. The solution was stirred at −20 °C for 15 min. and allowed to warm to ambient temperature and stirred for an additional 6 h. The solution was diluted with acetone (6 mL) and stirred for 30 min. Diethyl ether (40 mL) was added to precipitate triphenylphosphine oxide. The latter was removed by filtration through Celite™ 545 filter aid. The filtrate was washed successively with satd. aq. $NaHCO_3$ and brine (50 mL X 3). The solution was dried with anhydrous Na_2SO_4, filtered and the filtrate concentrated under reduced pressure to obtain the crude product. The product was purified by silica gel flash column chromatography on silica gel to give product as a yellow oil **25**: yield 55% (1.30 g); R_f = 0.63 (30% ethyl acetate : hexane). All the NMR values match with the reported data.[45]

3,4,7-Tri-*O*-benzyl-5-*O*-(2',3',4',6'-tetra-*O*-benzyl-α-D-glucopyranosyl)-D-gluchept-1-enone (26)

Compound **25** (1.20 g, 1.24 mmol) was dissolved by gentle warming in anhydrous benzene (3.0 mL). To this solution was added dry dimethyl sulfoxide (3.0 mL). To the clear solution was added anhydrous pyridine (99.5 µL, 1.24 mmol), trifluoracetic acid (47.3 µL, 0.62 mmol) and *N,N'*-dicyclohexylcarbodiimide (0.76 g, 3.70 mmol) in that order. The reaction was left to stir at room temperature for 18 h. After completion of reaction, which was monitored by TLC, benzene (10 mL) was added. The resulting crystalline dicyclohexylurea was removed by filtration and washed with benzene. The combined filtrates and washings were extracted with water (20 mL X 3) to remove dimethyl sulfoxide. The organic layer was dried over anhydrous Na_2SO_4, evaporated under reduced pressure, and subjected to flash column chromatography on silica gel with 1:6 ethyl acetate–hexane to give product as colorless viscous liquid **26**: yield 88% (1.05 g); silica gel TLC R_f = 0.72 (30% ethyl acetate : hexane); ^{1}H NMR (600 MHz, $CDCl_3$) δ 7.33–7.23 (m, 33H, aromatic), 7.17–7.15 (m, 2H, aromatic), 5.97 (m, 1H, H-1), 5.24 (m, 2H, =CH_2), 4.93 (d, *J* = 11 Hz, 1H, PhC*H*), 4.90–4.84 (m, 4H, PhC*H*, H-1'), 4.68 (dd, *J* = 12, 4.1 Hz, 2H, PhC*H*), 4.56 (dd, *J* = 12, 4.1 Hz, 2H, PhC*H*), 4.48 (d, *J* = 10.8 Hz, 1H, PhC*H*), 4.44–4.37 (m, 4H, PhC*H*, H-6a), 4,26 (d, *J* = 6.2 Hz, 1H, H-4), 4.18–4.24 (m, 3H, PhC*H*, H-6b), 4.09–4.06 (m, 2H, H-3', H-2), 3.93 (m, 1H, H-5'), 3.85 (dd, *J* = 6.2, 4.4 Hz, 1H, H-3), 3.79–3.74 (m, 2H, H-4', H-6a'), 3.54 (dd, *J* = 9.7, 3.7 Hz, 1H, H-2'), 3.45 (dd, *J* = 10.8, 1.8 Hz, 1H, H-6b'); ^{13}C NMR (150 MHz, $CDCl_3$): δ 204.40, 138.77, 138.53, 138.28, 138.19, 137.92, 137.91, 137.64, 134.92, 128.41, 128.34, 127.70, 127.63, 118.92, 99.72, 81.73, 80.64, 79.71, 79.71, 79.23, 75.64, 74.90,

74.55, 73.48, 73.20, 73.06, 70.74, 68.06 ppm; mass spectrum (HRMS), *m/z* = 969.4601 $(M+H)^+$, $C_{62}H_{64}O_{10}$ requires 969.4578.

3,4,9-Tri-*O*-benzyl-5-*O*-(2',3',4',6'-tetra-*O*-benzyl-α-D-glucopyranosyl)-D-gluco-octa-1,7-dienitol (27A)

To a cooled (−78 °C) solution of **26** (1.04 g, 1.07 mmol) in tetrahydrofuran (15 mL) was added of vinylmagnesium bromide (0.7 M) in tetrahydrofuran (4.57 mL, 3.20 mmol) dropwise. The reaction mixture was stirred for 1 h. at the same temperature. The reaction mixture was warmed to room temperature. Diethyl ether (30 mL) and aq. NH_4Cl (30 mL) were added to the reaction mixture. The organic layer was separated, washed with brine (50 mL X 2), and dried over anhydrous Na_2SO_4. The solvent was evaporated under reduced pressure and purification was performed by flash column chromatography on silica gel with 1:8 ethyl acetate–hexane to afford product as colorless viscous liquid **27A**: yield 93% (0.97 g); silica gel TLC R_f = 0.65 (30% ethyl acetate : hexane); ^1H NMR (600 MHz, $CDCl_3$) δ 7.40–7.23 (m, 31H, aromatic), 7.22–7.17 (m, 4H, aromatic), 6.30 (dd, *J* = 17.4, 10.6 Hz, 1H, H-7), 5.79 (ddd, *J* = 17.6, 10.4, 7.5 Hz, 1H, H-2), 5.59 (dd, *J* = 17.4, 1.7 Hz, 1H, H-8a), 5.37 (br dd, *J* = 17.3, 1.1 Hz, 1H, H-1a), 5.33 (d, *J* = 3.4 Hz, 1H, H-1'), 5.27 (ddd, *J* = 10.2, 6.8, 1.7 Hz, 2H, H-1b, H-8b), 5.01 (d, *J* = 10.9, 10.9 Hz, 2H, PhC*H*), 4.89 (d, *J* = 11.5 Hz, 2H, PhC*H*), 4.66–4.43 (m, 10H, PhC*H*, H-3), 4.29 (d, *J* = 11.7 Hz, 1H, PhC*H*), 4.11–4.03 (m, 2H, H-5, H-3'), 4.00–3.92 (m, 2H, H-5', H-4), 3.85 (brs, 1H, OH), 3.76–3.68 (m, 2H, H-4', H-9a), 3.64 (dd, *J* = 9.8, 3.5 Hz, 1H, H-2'), 3.55 (dd, *J* = 10.8, 2.8 Hz, 1H, H-6a'), 3.44 (dd, *J* = 10.7, 1.6 Hz, 1H, H-6b'), 3.36 (d, *J* = 8.9 Hz, 1H, H-9b). ^{13}C NMR (150 MHz, $CDCl_3$): δ 139.92, 138.86, 138.71, 138.60, 1338.38, 137.99, 137.97, 137.71, 135.78, 128.35, 128.30, 128.18, 128.11, 127.92, 127.75, 127.65, 127.58, 127.48, 127.43, 127.35, 127.24, 119.35, 1155.67, 97.01, 82.97, 81.77, 79.74, 79.37, 77.61, 77.49, 75.47, 74.93, 74.78, 74.32, 73.44, 73.02, 72.54, 70.77, 70.48, 67.81 ppm; mass spectrum (HRMS), *m/z* = 997.4899 $(M+H)^+$, $C_{64}H_{68}O_{10}$ requires 997.4891.

3,4,9-Tri-*O*-benzyl-5-*O*-(2',3',4',6'-tetra-*O*-benzyl-α-D-glucopyranosyl)-L-ido-octa-1,7-dienitol (27B)

Flash column chromatography on silica gel with 1:6 ethyl acetate–hexane afforded product as colorless liquid **27B**: yield 23% (0.24 g); silica gel TLC R_f = 0.72 (30% ethyl acetate : hexane); ^1H NMR (600 MHz, $CDCl_3$) δ 7.35–7.13 (m, 33H, aromatic), 7.04 (m, 2H, aromatic), 6.27 (dd, *J* = 17.3, 10.9 Hz, 1H, H-7), 5.81 (ddd, *J* = 17.3, 10.2, 8.3 Hz, 1H, H-2), 5.60 (dd, *J* = 17.4, 1.9 Hz, 1H, H-8a), 5.44 (d, *J* = 3.4 Hz, 1H, H-1'), 5.37 – 5.26 (m, 3H, H-1a, H-1b, H-8b), 4.98 (d, *J* = 10.8 Hz, 1H, PhC*H*), .4.93 (d, *J* = 11.0 Hz, 1H, PhC*H*), .4.84 (d, *J* = 10.8 Hz, 1H, PhC*H*), 4.80 (d, *J* = 10.8 Hz, 1H, PhC*H*), 4.60 (dd, *J* = 16.5, 11.3 Hz, 2H, PhC*H*), 4.49–4.33 (m, 8 H, PhCH), 4.25 (t, *J* = 8.3, 8.3 Hz, 1H, H-3), 4.05 (d, *J* = 1.8 Hz, 1H, H-5), 3.95–3.90 (m, 2H, H-4, H-3'), 3.84 (d, *J* = 9.2 Hz, 1H, H-9a), 3.77 (m, 1H, H-5'), 3.69–3.63 (m, 1H, H-4'), 3.54 (dd, *J* = 9.3, 4.6 Hz, 1H, H-2'), 3.39 (dd, *J* = 10.6, 2.7 Hz, 1H, H-6a'), 3.33–3.29 (m, 2 H, H-6b', H-9b), 2.97 (brs, 1H, OH); ^{13}C NMR (150 MHz, $CDCl_3$): δ 139.20, 138.81, 138.68, 138.59, 138.35, 137.93, 137.77, 137.20, 135.86, 128.28, 127.63, 127.54, 127.13, 120.06, 115.69, 94.33, 84.60, 81.93, 79.01, 77.90, 77.30, 78.15, 75.46, 74.46, 74.86, 74.67, 73.43, 72.78, 71.15, 70.44, 67.86 ppm; mass spectrum (HRMS), *m/z* = 997.4899 $(M+H)^+$, $C_{64}H_{68}O_{10}$ requires 997.4891.

(*1*D)-(1,3,4/2)-1,2-Di-*O*-benzyl-4-*C*-[(benzyloxy)methyl]-3-*O*-(2',3',4',6'-tetra-*O*-benzyl-α-D-glucopyranosyl)cyclohex-5-ene-1,2,3,4-tetrol (28A)

28A: yield 25% (0.25 g); silica gel TLC R_f = 0.5 (30% ethyl acetate : hexane); ^{1}H NMR (600 MHz, $CDCl_3$) δ 7.30–7.20 (m, 33H, aromatic), 7.19–7.11 (m, 2H, aromatic), 5.96 (dd, *J* = 10.2, 1.9 Hz, 1H, H-6), 5.69 (dd, *J* = 10.3, 1.8 Hz, 1H, H-5), 5.63 (d, *J* = 3.7 Hz, 1H, H-1'), 4.98 (d, *J* = 11.7 Hz, 1H, PhC*H*), 4.91–4.81 (m, 3H, PhC*H*), 4.77 (d, *J* = 10.9 Hz, 1H, PhC*H*), 4.67 (dd, *J* = 29.4, 11.7 Hz, 2H, PhC*H*), 4.59–4.43 (m, 6H, PhC*H*), 4.36 (d, *J* = 12.2 Hz, 1H, PhC*H*), 4.22 (m, 1H, H-1), 4.21–4.17 (m, 2H, H-2, H-3), 3.97 (t, *J* = 9.3 Hz, 1H, H-3'), 3.89 (m, 1H, H-5'), 3.70–3.63 (m, 2H, H-4', H-7b), 3.56 (ddd, *J* = 13.5, 10.2, 3.5 Hz, 2H, H-2', H-6a'), 3.49(dd, *J* = 10.5, 1.8 Hz, 1H, H-6b'), 3.39 (d, *J* = 9.1 Hz, 1H, H-7a), 3.22 (brs, 1H, OH); ^{13}C NMR (150 MHz, $CDCl_3$): δ 139.10, 138.66, 138.34, 138.31, 138.10, 137.96, 137.78, 130.75, 130.31, 128.35, 128.33, 128.27, 128.17, 128.08, 127.92, 127.84, 127.77, 127.65, 127.55, 127.41, 127.66, 126.92, 97.02, 81.77, 80.82, 80.10, 79.60, 77.54, 75.48, 74.95, 74.12, 73.49, 73.10, 72.98. 72.74, 71.50, 68.10 ppm; mass spectrum (HRMS), *m/z* = 991.4418 $(M+Na)^+$, $C_{62}H_{64}O_{10}$ requires 991.4397.

(*1*D)-(1,3,4/2)-1,2-Di-*O*-benzyl-4-*C*-[(benzyloxy)methyl]-3-*O*-(2',3',4',6'-tetra-*O*-benzyl-α-D-glucopyranosyl)cyclohex-5-ene-1,2,3,4-tetrol (28B)

28B: yield 25% (60.0 mg); silica gel TLC R_f = 0.5 (30% ethyl acetate : hexane); ^{1}H NMR (600 MHz, $CDCl_3$) δ 7.35–7.15 (m, 35H, aromatic), 5.74 (ddd, *J* = 22.2, 10.4, 1.9 Hz, 2H, H-5, H-6), 5.32 (d, *J* = 3.8 Hz, 1H, H-1'), 5.04 (d, *J* = 12.0 Hz, 1H, PhC*H*), 4.93 (d, *J* = 10.9 Hz, 1H, PhC*H*), 4.87–4.76 (m, 3H, PhC*H*), 4.42–4.64 (m, 9H, PhC*H*), 4.27 (dt, *J* = 7.0, 1.8 Hz, 1H, H-1), 4.16 (dd, *J* = 10.5, 7.1 Hz, 1H, H-2), 3.95–3.89 (m, 2H, H-3, H-3'), 4.93 (d, *J* = 10.9 Hz, 1H, PhC*H*), 4.93 (d, *J* = 10.9 Hz, 1H, PhC*H*), 3.73 (d, *J* = 9.4 Hz, 1H, H-7a), 3.67 (d, *J* = 9.4 Hz, 1H, H-7b), 3.61–3.51 (m, 4H, H-2', H-4', H-6a', H-6b'), 3.40 (brs, 1H, OH); ^{13}C NMR (150 MHz, $CDCl_3$): δ 139.37, 138.72, 136.64, 136.21, 138.13, 137.99, 137.80, 132,14, 128.41, 128.38, 128.37, 128.32, 128.17, 128.10, 128.06, 128.03, 127.90, 127.80,, 127.76, 127.73, 127.62, 127.56, 127.47, 126.99, 126.95, 126.66, 99.37, 84.31, 81.67, 80.95, 80.46, 79.24, 77.24, 75.52, 75.12, 75.05, 74.37, 73.62, 73.58, 73.53, 72.41, 71.33, 71.11, 68.51, 29.73 ppm; mass spectrum (HRMS), *m/z* = 991.396 $(M+Na)^+$, $C_{62}H_{64}O_{10}$ requires 991.4397.

(*1*D)-(1,3,4/2)-1,2-Di-*O*-benzyl-4-*C*-[(benzyloxy)methyl]-4-*O*-carbamoyl-3-*O*-(2',3',4',6'-tetra-*O*-benzyl-α-D-glucopyranosyl)cyclohex-5-ene-1,2,3,4-tetrol (29)

A solution of **28A** (0.24 g, 0.25 mmol) in dichloromethane (10 mL) was cooled at 0 °C and treated dropwise with trichloroacetyl isocyanate (60 µL, 0.50 mmol). The reaction mixture was stirred for 30 min. at the same temperature and evaporated. The residue was dissolved in methanol (10 ml) and water (1 ml), was cooled to 0 °C and treated with potassium carbonate (0.07 g, 0.49 mmol). The reaction mixture was stirred for 2 h. at that temperature and warmed to room temperature and again stirred for another 2 h. After completion of the reaction, methanol was evaporated and the aq. solution. was diluted with water (10 mL) and extracted with dichloromethane (20 mL X 3). The organic layer was separated washed with

brine (10 mL X 3), dried over anhydrous Na_2SO_4. The solvent was evaporated under reduced pressure and purification was performed by flash column chromatography on silica gel with 1:3 ethyl acetate–hexane to afford product as colorless liquid **29**: yield 85% (0.21 g); silica gel TLC R_f = 0.25 (30% ethyl acetate : hexane); ^{1}H NMR (600 MHz, $CDCl_3$) δ 7.36–7.20 (m, 33H, aromatic), 7.16–7.14 (m, 2H, aromatic), 6.32 (dd, *J* = 10.2, 1.9 Hz, 1H, H-6), 6.01 (dd, *J* = 10.3, 1.8 Hz, 1H, H-5), 5.53 (d, *J* = 3.7 Hz, 1H, H-1'), 5.07 (d, *J* = 11.7 Hz, 1H, PhC*H*), 4.92 (m, 2H, PhC*H*), 4.86 (d, *J* = 11.0 Hz, 1H, PhC*H*), 4.65 (dd, *J* = 11.4, 9.0 Hz, 2H, PhC*H*), 4.59–4.56 (m, 2H, PhC*H*), 4.52–4.45 (m, 4H, 2 PhC*H*), 4.35 (d, *J* = 12.0 Hz, 1H, PhC*H*) 4.28–4.23 (m, 3H, H-1, H-2, H-3), 4.14–4.08 (m, 3H, H-3', H-7a, H-7b), 4.02 (m, 1H, H-5'), 3.68 (t, *J* = 9.6, 9.6 Hz, 1H, H-4'), 3.61 (dd, *J* = 10.2, 3.0 Hz, 1H, H-6a'), 3.54 (dd, *J* = 9.6, 3.6 Hz, 1H, H-2'), 3.50 (d, *J* = 10.2 Hz, 1H, H-6b'). ^{13}C NMR (150 MHz, $CDCl_3$): δ 155.39, 139.32, 138.84, 138.30, 138.24, 138.17, 138.13, 137.87, 130.68, 129.67, 128.41, 128.39, 128.36, 128.31, 128.25, 128.19, 128.12, 128.05, 127.99, 127.93, 127.90, 127.77, 127.69, 127.57, 127.53, 127.39, 127.07, 126.97, 98.13, 81.53, 81.09, 80.50, 79.77, 79.75, 77.77, 75.93, 75.47, 75.16, 74.43, 73.47, 73.16, 72.50. 71.76, 70.90, 69.78, 68.51 ppm; mass spectrum (HRMS), *m/z* = 1034.4463 $(M+Na)^+$, $C_{63}H_{65}NO_{11}$ requires 1034.4455.

(*1*D)-(1,3,4/2)-1,2-Di-*O*-benzyl-6-[(benzyloxycarbonyl) amino]-4-[(benzyloxy)methyl]-3-*O*-(2',3',4',6'-tetra-*O*-benzyl-α-D-glucopyranosyl) cyclohex-4-ene-1,2,3-triol (30)

Trifluoracetic anhydride (56.0 µL, 0.39 mmol) was added to a solution of carbamate **29** (0.20 g, 0.19 mmol) and triethylamine (165 µL, 1.19 mmol) in dry tetrahydrofuran (10 mL) and was cooled to 0 °C. The resulting mixture was slowly warmed to room temperature and stirred for 1 h. In a separate flask, sodium hydride suspension in 60% mineral oil (0.01 g, 0.39 mmol) was added to a solution of benzyl alcohol (41.0 µL, 0.39 mmol) in dry tetrahydrofuran (2 mL) at 0 °C. After 1 hr, the solution of sodium benzyloxide was added to the generated isocyanate and the reaction progress was followed by TLC. After 24 h. volatiles are removed under reduced pressure. The reaction mixture was diluted with water (10 mL) and extracted with dichloromethane (10 mL X 4). The organic layer was separated washed with brine (10 mL X 2), dried over anhydrous Na_2SO_4. The solvent was evaporated under reduced pressure and purification was performed by flash column chromatography on silica gel with 1:5 ethyl acetate–hexane to afford product as colorless liquid **30**: yield 60% (0.13 g); silica gel TLC R_f = 0.43 (30% ethyl acetate : hexane); ^{1}H NMR (600 MHz, $CDCl_3$) δ 7.23–7.11 (m, 40H, aromatic), 5.92 (d, *J* = 3.0 Hz, 1H, H-5), 5.49 (d, *J* = 9.7 Hz, 1H, N*H*), 5.10–5.05 (m, 3H, H-1', cbz), 4.79–4.71 (m, 3H, H-6, PhC*H*), 4.68–4.57 (m, 6H, PhC*H*), 4.51–4.36 (m, 6H, PhC*H*), 4.29 (br d, *J* = 4.8 Hz, 1H, H-3), 4.25 (d, *J* = 12.6 Hz, 1H, H-7a), 4.04 (dd, *J* = 4.8, 1.9 Hz, 1H, H-2), 3.94 (d, *J* = 12.6 Hz, 1H, H-7b), 3.90-3.87 (m, 2H, H-3', H-5'), 3.76 (t, *J* = 4.8, 4.8 Hz, 1H, H-1), 3.68 (t, *J* = 9.6 Hz, 1H, H-4'), 3.63 (dd, *J* = 10.6, 2.9 Hz, 1H, H-6a'), 3.56 (dd, *J* = 9.8, 3.6 Hz, 1H, H-2'), 3.47 (dd, *J* = 10.6, 1.9 Hz, 1H, H-6b'). ^{13}C NMR (150 MHz, $CDCl_3$): δ 156.23, 138.71, 138.41, 138.23, 138.01, 137.93, 137.92, 136.65, 135.29, 128.49, 128.46, 128.41, 128.36, 128.34, 128.28, 127.99, 127.98, 127.92, 127.86, 127.74, 127.69, 127.59, 127.52, 127.49, 127.35, 97.58, 81.98, 79.52, 77.67, 75.93, 75.61, 75.33, 74.91, 73.96, 73.49, 73.03, 71.81, 71.77, 71.26, 71.03, 70.95, 68.16, 66.61, 46.54 ppm; mass spectrum (HRMS), *m/z* = 1124.4922 $(M+Na)^+$, $C_{70}H_{71}NO_{11}$ requires 1124.4925.

L-chiro-Inisitol-1-amino-1,5,6-trideoxy-4-*O*-(α-D-glucopyranosyl)-5-(hydroxymethyl) or 4-*α*-glycoside derivative of validamine (7)

Compound **30** (40.0 mg, 0.04 mmol) was dissolved in 10 mL of methanol and 20% $Pd(OH)_2/C$ on carbon (20.0 mg) was added. The mixture was stirred for 16 h. under hydrogen (1 atm.). The catalyst was filtered away through a plug of Celite® 545 and washed with methanol (5mL). The combined filtrate and washings were concentrated to dryness and the residue was passed through reverse phase C-18 silica gel (washed with water) to afford **7** as a white solid: yield quantitative (5.00 mg); ^{1}H NMR (600 MHz, D_2O) δ 5.09 (d, *J* = 3.84 Hz, 1 H), 4.21 (m, 1 H), 3.92 (m, 2 H), 3.75–3.52 (m, 8 H), 3.35–3.32 (m, 1H), 2.13 (m, 1H), 1.71–1.55 (m, 2H). ^{13}C NMR (151 MHz, D_2O): δ 96.30, 73.06, 72.87, 72.69, 70.93, 69.04 (2C), 66.14, 62.37, 60.25, 48.94, 36.62, 21.63 ppm; mass spectrum (HRMS), *m/z* = 340.1599 $(M+H)^+$, $C_{13}H_{25}NO_9$ requires 340.1600.

α-D-Glucopyranoside, 4-amino-5,6-dihydroxy-2-(hydroxymethyl)-2-cyclohexen-1-yl or 4-*α*-glycoside derivative of valienamine (8)

Ammonia was condensed into a solution of **30** (60.0 mg, 0.05 mmol) in tetrahydrofuran (5 ml) using a dry ice cooled cold finger apparatus. The solution was treated with sodium in small pieces, until a blue color in the solution persisted. After stirring for 10 min. at –78 °C temperature the mixture was treated with NH_4Cl (100 mg), stirred at room temperature overnight and evaporated. The residue was extracted with methanol, filtered, and evaporated. The residue (20.0 mg) was adsorbed on 3 mL of neutral *Dowex 50-WX-8* (washed with water). After washing with water (10 mL), elution with 2% aqueous ammonia gave **8** as a white solid: yield quantitative (5.00 mg); ^{1}H NMR (600 MHz, D_2O): δ 5.71 (d, *J* = 4.2 Hz, 1H), 5.26 (d, *J* = 3.9 Hz, 1H), 4.16–4.06 (m, 3H), 3.93–3.85 (m, 3H), 3.71–3.58 (m, 3H), 3.50–3.40 (m, 2H), 3.27–3.23 (m, 1H). ^{13}C NMR (151 MHz, D_2O): δ 142.85, 117.37, 97.76, 75.27, 72.65, 72.63, 71.09, 70.14, 69.17, 66.40, 61.34, 60.31, 48.57 ppm; mass spectrum (HRMS), *m/z* = 338.1440 $(M+H)^+$, $C_{13}H_{23}NO_9$ requires 338.1446.

Protein purification

The expression construct of *Sco* GlgE1-V279S (pET32-*Sco* GlgE1-V279S),[27] that encodes for a non-cleavable C-terminal polyhistidine tagged protein, was used to transform T7 express E. coli cells. The large-scale cultures were grown at 37 °C in LB media with 264 mM concentration of carbenicillin. When $O.D_{600nm}$ reached 0.6, cultures were cooled to 16 °C and cells were induced by the addition of 1 mM Isopropyl β-D-1-thiogalactopyranoside. After 16 hours of induction, cells were harvested by centrifugation and resuspended in a lysis buffer consisting of 20 mM Tris pH 7.5, 500 mM NaCl, 10 % glycerol, 0.5 mM imidazole and 0.3 mM tris(2-carboxyethyl) phosphine (TECP). The cell suspension was incubated on ice with lysozyme and DNase I for 30 min and lysed by sonication. The resulting lysate was clarified by centrifugation and subjected to a 5 mL metal affinity cobalt column that had been equilibrated with lysis buffer. The unbound protein was washed by passing 25 column volumes of lysis buffer through the

column and *Sco* GlgE1-V279S was eluted isocratically with the elution buffer of 20 mM Tris pH 7.5, 500 mM NaCl, 150 mM imidazole and 0.3 mM TCEP. The excess salt and imidazole were removed from *Sco* GlgE1-V279S by overnight dialysis against a buffer consisting of 20 mM Tris pH 7.5, 150 mM NaCl and 0.3 mM TCEP.

Inhibition studies

The inhibition studies for **7** and **8** were performed separately by using EnzChek Phosphate Assay Kit. Prior to the assay, stock solutions of 1 mM MESG, 20 mM concentrations of **7** and **8** (dissolved dH_2O) were prepared and stored at -20 °C. In the assay, all the reactions were carried out in a 96-well format, 50 µL reaction volume at 25 °C for 20 minutes in a continuous manner. The reactions were initiated by addition of 50 nM *Sco* GlgE1-V279S to the reaction mixture consisting of 20 mM Tris pH 7.5, 150 mM NaCl, 500 nM MESG, 0.25 U PNP, 0.5 mM glycogen (as maltose acceptor) and 250 µM M1P.[27,52] In the various reactions, the compound **8** concentration was varied from 0 to 1000 µM, except in the positive control that lacked inhibitor, and the negative control that lacked enzyme. All of the reactions were performed in triplicate using a Synergy H4 plate reader (Bio Tek) to measure the absorbance at 360 nm. The percent enzymatic activity was calculated by using the equation $(V/V_0) \times 100$, where V and V_0 denote the rates of the inhibited and uninhibited enzyme (positive control), respectively. The percent enzymatic activity vs inhibitor concentration was plotted using Prism 8 and the equation $y = 100/ (1+(IC_{50}/x)^{Hillslope})$ was used to determine the IC_{50}. Using this assay, 100 µM concentration of both **7** and **8** were tested separately against *Sco* GlgE1-V279S. Dose-response experiments for **8** were performed as described above while varying the concentration of **8**.

Crystallization of *Sco* GlgE1-V279S complexes

Prior to the experiment, 20 mM aqueous solutions of **7** and **8** were prepared. The protein-compound mixture was prepared by mixing the *Sco* GlgE1-V279S with each compound separately to a final concentration as 8 mg/mL[51] of *Sco* GlgE1-V279S and 10 mM of the respective compound. The hanging drop vapor diffusion method was used for the crystallization and each crystallization drop consisted with 2 µL of *Sco* GlgE1-V279S/compound mixture and 2 µL of the well solution (0.2 mM Sodium citrate pH 7 and 10 % PEG 3,350).[45] The crystallization drop was equilibrated against 100 µL of the well solution and crystals were formed within 3 days. Following crystal formation, an additional 4 µL of the appropriate 20 mM compound stock was added to the drop and incubated for an additional 12 hours. Crystals were cryoprotected by adding 4 µL of 50% PEG 2000 to the crystallization drop, and crystals were flash-cooled using liquid nitrogen in preparation for the cryo-crystallographic experiments.

X-ray Diffraction experiments

The LS-CAT beamline at Advanced Photon Source of Argonne National Labs, IL was used to perform the X-ray diffraction experiments. The X-ray diffraction data corresponding to the *Sco* GlgE1-V279S/**7** and *Sco* GlgE1-V279S/**8** complexes were indexed and reduced, using DIALS, iMosflm, and Scala in the CCP4

suite. The refinements were carried out by using PHENIX, and the previously published *Sco* GlgE1-V279S in complex with maltose-C-phosphonate (RCSB accession number 4U31) was used for difference Fourier analysis to calculate phases and difference maps prior to manual and computational refinement.[68] The visualization and manual refinements of the structures were carried out using COOT.[69] The final occupancy of each ligand was changed manually and then refined in PHENIX.

Results And Discussion

Before synthesizing the target pseudodisaccharides, we synthesized valienamine (**6**) from commercially available D-(+)-glucose (**9**) to obtain spectroscopic diastereoselectivity metrics for the intermediates afforded by the stereoselective addition of vinylmagnesium bromide to ketone **15**, Scheme 2. The spectral analysis of the intermediates **16A**, **16B**, **17A**, and **17B** proved critical in analyzing the desired diastereomer of the maltosyl analogues. Compound **15** was obtained starting from **9** in seven steps that involved Wittig olefination and Moffatt oxidation (Scheme S1 in Supporting Information).[27,35,36] The key step in the synthesis is the diastereoselective addition of vinylmagnesium bromide to enone **15** to afford separable diastereomers **16A** and **16B** (9:1). The high selectivity for the conformer **16A** over the conformer **16B** can be explained by Cram's-chelate TS model.[37,38] According to previous reports, the torsional strain in enone **15** implies a staggered conformation in the TS where the nucleophile attacks preferentially from the *si* face, Scheme 2.[34,37,39] Moreover, the downfield shift of the C(6)-OH signal of **16A** relative to the chemical shift of C(6)-OH of **16B** indicated a strong intramolecular H-bond (six-membered ring) to C(4)-OBn in **16A** and a five-membered H-bond to C(9)-OBn in **16B**, Figure 3.

Although, there is little to distinguish the relative stereochemistry of **16A** and **16B**, after the intramolecular ring closing metathesis (RCM), Kapferer et al. assigned the absolute stereochemistry of the carbasaccharides **17A** and **17B** by comparing the spectroscopic data and Nuclear Overhauser Effect (NOE) experiments.[34] Finally, **17A** was converted to valienamine (**6**) in three steps involving Ichikawa rearrangement, (Scheme S1 in Supporting Information).[40] The spectral data of all the intermediates were found nearly identical to the previously reported data (Supporting Information).[34,41]

After successfully synthesizing valienamine (**6**), we synthesized the pseudodisaccharides **7** and **8** starting from D-(+)-maltose, Scheme 3, and the intermediates of Scheme 2 were used to assign the diastereomers. D-(+)-maltose (**20**) was peracetylated with acetic anhydride followed by the treatment with *p*-thiocresol and boron-trifluoride diethyl etherate to generate a peracetylated β-thiomaltoside.[42] Subsequently, deacetylation under Zemplén conditions afforded glycoside **22** followed by benzylation to afford perbenzylated thiomaltosid e (**23**) in 85% yield.[43] We treated thiomaltoside **23** with *N*-bromosuccinimide (NBS) in acetone:water (9:1) to obtain the reducing sugar **24**.[44] Wittig methylenation of **24** using methyltriphenylphosphonium bromide in the presence of *n*-butyl lithium afforded alkene **25** in 55% yield.[45] After that, the secondary alcohol **25** was oxidized under Moffatt oxidation conditions to afford ketone **26** in 90% yield.[36] Compound **26** was subjected to the stereoselective addition using

vinylmagnesium bromide in dry THF to afford diastereomeric dienes **27A** and **27B** in a 4:1 ratio, respectively (Scheme 3).

The ^{1}H NMR chemical shift values and coupling constants of the epimers **27A** and **27B** were found to be comparable with the ^{1}H NMR chemical shift values and the coupling constants of the epimers **16A** and 16B (Table 1). Although the chemical shift of the terminal alkenyl protons in **27A** (Ha-C(8) 5.59 ppm, Hb-C(8) 5.27 ppm) and **27B** (Ha-C(8) 5.60 ppm, Hb-C(8) 5.30 ppm) appear in the same range as the respective terminal alkenyl protons in **16A** (Ha-C(8) 5.47 ppm, Hb-C(8) 5.19 ppm), and **16B** (Ha-C(8) 5.45 ppm, Hb-C(8) 5.23 ppm) the C(6)-OH signals of the maltosyl diastereomers followed the same trend as the C(6)-OH signals of the glucosyl diastereomers *vida supra*. The observed *J*(9a, 9b = 8.9 Hz) values for **27A** are smaller than the *J*(9a, 9b = 9.2 Hz) values for **27B**. Indeed, a similar pattern is noticed in the glucosyl dienes suggesting that **27A** and **27B** possess the same conformation as **16A** *J*(9a, 9b = 8.7 Hz) and **16B** *J*(9a, 9b = 9.3 Hz) respectively. However, the exact stereochemistry of the diastereomers **27A** and **27B** could not be confidently confirmed using only the ^{1}H NMR chemical shift and *J* values.

Complete structure elucidation of the desired epimer was achieved by further subjecting the dienes **27A** and **27B** to RCM using Grubb's 1st generation catalyst, Scheme 4. The reaction was optimized by using various conditions to improve the yield, Table 2. The highest yield (25%) was obtained using Grubb's first-generation catalyst under DCM reflux conditions.

The ^{1}H NMR chemical shift values of **28A** and **28B** were compared with the α-glycosylated aminocarbasugars **17A** and **17B**. The alkenyl protons in **28A** (H-C(5) 5.69 ppm, H-C(6) 5.92 ppm) and **28B** (H-C(5) 5.74 ppm, H-C(6) 5.74 ppm) appear at the exact same chemical shifts as the respective alkenyl protons in **17A** (H-C(5) 5.69 ppm, H-C(6) 5.96 ppm), and **17B** (H-C(5) 5.74 ppm, H-C(6) 5.74 ppm) giving a clear indication of matching relative configurations as per literature.[34] The C-atoms carrying an equatorial substituent, especially oxy groups, resonate at a higher field than those with axial substituents, justifying the ^{13}C NMR chemical shifts for C(4) of **28A** (73.10 ppm) and **28B** (75.07 ppm) (Table 3).[46] A similar trend in the ^{13}C NMR chemical shift values was also observed in the glucosyl diastereomers

The synthesis continued with the protection of the tertiary alcohol of **28A** with trichloroacetyl isocyanate in dichloromethane (DCM) at 0 °C, followed by hydrolysis with K_2CO_3 in aqueous MeOH giving an 85% yield of the carbamate **29**. Compound **29** was subjected to an Ichikawa rearrangement[40] that proved useful in the synthesis of valienamine (**6**).[34] Here, the dehydration of **29** with trifluoroacetic anhydride (TFAA) and Et_3N at –20 °C formed an intermediate allylic cyanate that underwent a spontaneous [3,3]-sigmatropic rearrangement to afford the isocyanate. The isocyanate was treated in situ with 60% NaH in mineral oil and benzyl alcohol solution to yield protected maltosyl valienamine analog **30** in 60% overall yield, Scheme 5.

Kozikowski et al. reported that hydrogenation of substituted cyclohexenes yields two diastereomers where the major isomer has the hydroxy methylene at the equatorial position.[47] However, hydrogenation of **30** using 20% $Pd(OH)_2/C$ afforded a single isomer **7** in a quantitative yield. We compared the ^1H NMR chemical shift values of the obtained compound with reported validamine (**2a**)[48] and epi-validamine (**2b**)[49] to determine the stereochemistry at C(5), Table 4. Although the proton chemical shift value of **7** at C(5) is similar to **2b**, no sound conclusion can be derived due to difference in the chemical environment. Therefore, we compared the C(6) protons of **7** with the C(6) protons of **2a** and **2b**. For epi-validamine, the Ha-(6) and Hb-(6) appear at different chemical shifts (1.78 ppm and 2.11 ppm) whereas for validamine (**2a**), both the C(6) protons appear as a multiplet (1.74-1.59 ppm). After the spectral analysis of **7**, we observed a similarity in the chemical shifts and peak splitting pattern of the C(6) protons (1.71-1.55 ppm) to validamine (**2a**), thereby, confirming that the hydroxy methylene in target compound **7** is at the equatorial position. Finally, the benzyl carbamate **30** was subjected to deprotection under Birch reduction conditions to afford target compound **8**.

Inhibition studies were carried out using **7** and **8** separately against *Sco* GlgE1-V279S. The maltosyltransferase activity of *Sco* GlgE1-V279S using M1P was determined by coupling with purine nucleoside phosphorylase (PNP), using the previously published method.[27] Enzyme activity of *Sco* GlgE1-V279S decreased by 32 % at 100 μM concentration of **8**, but **7** failed to exhibit any inhibition of *Sco* GlgE1-V279S. Similarly, a 1 mM concentration of **7** also failed to inhibit the enzyme. Therefore, only compound **8** was used for dose-dependence studies at concentrations between 0 and 1000 μM. Using the data plotted in Figure 4, the IC_{50} of compound **8** was determined to be 484 ± 51 μM. Unfortunately, lack of **8** solubility beyond 1 mM prevents inhibitor saturation of *Sco* GlgE1-V279S and a more accurate IC_{50} determination of the compound. However, as the two highest inhibitor concentrations clearly exhibit enzyme activity below 50 % when normalized with the rate of the uninhibited enzyme, the calculated IC_{50} for compound **8** is reasonably accurate.

The X-ray crystal structures of *Sco* GlgE1-V279S/**7** and Sco GlgE1-V279S/**8** complexes were pursued to gain insight regarding the lack of efficacy of **7** and evaluate the role of ring flattening in affording the inhibitory activity of **8**. The results of the X-ray diffraction experiment afforded refinement of the *Sco* GlgE1-V279S/**7** and Sco GlgE1-V279S/**8** complex structures to resolutions of 1.75 Å and 1.78 Å, respectively. The evidence from the $2F_O$-F_C composite omit maps (Figure 5) demonstrate the presence of each compound in the M1P binding site. In addition to the strong density observed for both **7** and **8** in the respective structures, the GlgE1-V279S/**7** complex also exhibits a well-ordered spherical density located 3.2 Å from the exocyclic amine moiety of **7** that we have modeled as a chloride ion. Based on the proximity of the C(1) ammonium moiety to Glu 423 in both structures, the presence of the chloride ion in

the *Sco* GlgE1-V279S/**7** complex structure, and the pH of the crystallization condition (pH 7.5), we expect the “amine” moiety of **7** (and **8**) to harbor a positively charged ammonium moiety and the following discussion will reflect that assumption.

The compounds bound within the M1P binding sites in each structure provide important information about enzyme-compound interactions and the geometry of the compounds within the active site. In both enzyme-compound structures, the interactions of the glucose moiety bound within the -2 subsite are the same as that observed in previously published *Sco* GlgE1-V279S/inhibitor complex structures.[50-53] However, interactions between the carbocycle moieties and the amino acid residues forming the -1 subsite differ significantly from each other. In the *Sco* GlgE1-V279S/**7** complex, the interactions are similar to those observed in the substrate-bound (M1P and maltose) and substrate-mimic (MCP) complexes because the saturated carbocycle in **7** maintains the expected chair conformation. Specifically, the C(2)-OH and C(3)-OH functional groups form a bidentate hydrogen-bonded interaction with Asp 480, which is a unique feature to the GH13 family of proteins and has been observed previously in GlgE (Figure 6A).[54,55] In addition, the C(2)-OH forms a hydrogen bond with the sidechain nitrogen atom/NH1 of Arg 392.

An unexpected difference between the *Sco* GlgE1-V279S/**7** complex structure and other complexes of disaccharide-like compounds is the rotation of the Asp 394 side chain away from the substrate analog. As this residue is known to form a hydrogen bond with the C6-OH group on incoming saccharides to allow positioning for nucleophilic attack on the anomeric carbon, it was anticipated to form the same hydrogen bond with **7**. However, the superimposed active sites of *Sco* GlgE1-V279S/**7** and *Sco* GlgE1/Maltose (PDB:3ZT5)[50] complexes (Figure 6B) clearly highlight χ2 dihedral rotation in Asp 394. This is exhibited unambiguously by the $2F_O$-F_C composite omit map density contoured at 1.5σ (Figure 7). The reason for this movement of Asp 394 appears to derive from steric hindrance with atom C(1) of **7**, apparently due to the ionic attraction between the C(1) ammonium moiety and the Glu 423 side chain. Since the crystals were grown at pH 7.5, the Asp side chains would be expected to be in the carboxylate form and harbor a negative charge, it is likely that has this charge attraction has shifted the carbocycle closer to Glu 423 than in other *Sco* GlgE1-V279S complexes. Inspection of the interaction network in this area illustrates that the side chains of Trp 281 and Tyr 251 form hydrogen bonds with each of the opposing aspartate side chains. Importantly, the Arg 392 side chain is positioned near the two aspartates and forms hydrogen bonds of 2.7 and 3.5 Å with Asp 394 and Asp 320, respectively. In apparent contrast to those stabilizing interactions, the 2.4 Å distance between O(D1) atoms of Asp 320 and Asp 394 represent the only possibly destabilizing interaction in this region. However, the very short distance between those atoms can be rationalized if either of the two side chains is protonated and the O(D1) atoms in those residues are using that hydrogen in a low barrier hydrogen bond. It is suspected that the

steric hindrance producing this energetically unfavorable repositioning of Asp 394 significantly limits the inhibitory activity of compound **7**.

When inspecting the *Sco* GlgE1-V279S/**8** complex, the amino acid residues forming the -1 subsite are consistent with previous *Sco* GlgE1-V279S complexes and do not undergo the structural change observed in the compound **7** complex. This is due to the expected structural differences observed compound **8** resulting from the presence of the sp^2 hybridized carbons at positions 5 and 6 in the carbocycle. The ring exhibits a flattened conformation that differs significantly from the chair conformation in **7** (Figure 8). This changes the hydroxyls at positions C(2) and C(3) from equatorial positions in **7** to axial positions in **8,** while the ammonium on C1 takes a more equatorial orientation that positions the ammonium group within 2.6 Å of the Glu 423 side chain carboxylate. These significant conformational differences in **8** mirror anticipated changes in the substrate during the enzymatic reaction. The C(3)-OH forms one of two hydrogen bonded interactions with the side chain of the Asp 394 nucleophile. The other hydrogen bond donor in this bidentate interaction is the C(7)-OH, whose location is nearly identical in both the **7** and **8** complex structures (Figure 8). Indeed, all previously published structures of GlgE with any hexose analog have a hydroxyl at this position that interacts directly with the enzyme nucleophile.[50,52] Although speculative, such a bidentate interaction could be envisioned to stabilize a $^3H_4$ or $B_{2,5}$-TSs in the enzyme catalyzed reaction. We note some studies have suggested that reactions catalyzed by this enzyme class proceed through a $^4C_1 \rightarrow {}^4H_3$-TS $\rightarrow {}^1S_3$ conformational itinerary leading to a $^4C_1$ enzyme-bound intermediate. [56,57] On the other hand, kinetic isotope effect studies have suggested a $^{2,5}B$ TS could be at play for some GH13 enzymes.[58] Others have noted the same data could be interpreted as a $^4C_1 \rightarrow {}^3S_1 \rightarrow {}^3H_4$-TS.[59] While more recently it was proposed *S. cerevisiae* α-glucosidase passes through a $^4H_3$ TS.[60] Further support of the $^3H_4$ or $B_{2,5}$-TSs hypothesis is derived from inspection of other GH13 enzymes in complex with acarbose, which is a tetrasaccharide possessing an *N*-glycosidic linkage that functions as an inhibitor of a-amylases. Inspection of available GH13 enzymes in complex with acarbose or acarbose-derived oligosaccharides (accession codes: 4B9Z, 4E2O, 6GXV, and 6LGE) show that the *N*-glucosyl moieties in these structures maintain a chair conformation with C(2)-OH and C(3)-OH in equatorial positions. This difference is likely due to the enzyme/acarbose complex resembling the Michaelis complex rather than mimicking a reaction intermediate as we propose for compound **8**.[61-64]

The ammonium moieties in both compounds form polar interactions with the side chain of the General acid/base, Glu 423. This interaction is consistent with the role of Glu 423 in protonating the OH leaving group during the first catalytic step and is likely stabilizing the complex due to the charge complementary between Glu 423 and the ammonium moieties. The difference in polar bond distances is a function of the ring flattening in **8** that both affords closer approach of the ammonium to Glu 423 while avoiding steric hindrance with Asp 394 (Figure 6A and Figure 8). This shorter polar bond distance and lack of movement in Asp 394 may be the major factor defining the differences in affinity observed for **7** and **8**. Additionally, in the *Sco* GlgE1-V279S/**7** complex, the well-ordered chloride ion appears to form ionic interactions with

the nitrogen atom of **7** and the side chain nitrogen atom of Lys 355. However, these interactions are rather long so likely contribute little to the binding affinity of **7**.

The active site comparison of both structures (Figure 9) indicates an upward shift in the carbocycle ring of compound **8**. Also, we observed some minor shifts in the side chains of Lys 355, Arg 392, Asp 394 and Glu 423, but these are within coordinate error. The superposition shown in Figure 6 also highlights the significant rotation of the χ2 dihedral observed in the *Sco* GlgE1-V279S/**7** complex. When measuring the χ1 dihedral angle (between Cα and Cβ atoms) of Asp 394 in GlgE1-V279S/**8** and *Sco* GlgE1-V279S/**7**, we identified a 119.4° dihedral difference. Due to this bond rotation, Asp 394 in *Sco* GlgE1-V279S shifts away from the substrate binding site and does not form any direct interaction with **7** (Figure 6A). In addition to the speculated low-barrier hydrogen bond with Asp 320, the carbonyl group of Asp 394 was further stabilized by formation of hydrogen bonds with the side chain nitrogen atom/NH1 of Arg 392 and the indole of Trp 281.

The previous studies relating to the synthesis and characterization of zwitterionic pyrrolidine-phosphonates showed that such compounds are reasonable mimics of the TSs formed during the enzymatic reaction. Out of those zwitterionic pyrrolidine-phosphonates, the methyl phosphonate pyrrolidine (MPP) is the most potent inhibitor against *Sco* GlgE1-V279S exhibiting an equilibrium dissociation constant (K_i) of 45 ± 4 μM.[52] The comparison of the active sites (Figure 10) of *Sco* GlgE1-V279S/**8** and *Sco* GlgE1-V279S/MPP (PDB:5VT4) clearly indicates interactions between GlgE residues forming the -2 subsite and the glucose moiety bound within that site are conserved in all the previously published GlgE structures. When comparing the -1 subsite of both structures, the pyrrolidine ring of *Sco* GlgE1-V279S/MPP complex and the flattened carbocycle moiety of *Sco* GlgE1-V279S/**8** complex mimic some aspects of the enzyme substrate conformations adopted during the formation of the first TS. Specifically, the hydrogen bonded interactions that form between the C(7)-OH hydroxyl and the carbonyl oxygen/OD1 of Asp 394 are identical for both *Sco* GlgE1-V279S/MPP and *Sco* GlgE1-V279S/**8** complexes. However, the role of Glu 423 as both an acid and a base in the enzymatic reaction affords different interactions in these two complexes with the side chain of Glu 423 forming a hydrogen bond with the negatively charged phosphonate in the MPP complex and an ionic interaction with the positively charged ammonium of compound **8**.

Further consideration of the *Sco* GlgE1-V279S/**8** and *Sco* GlgE1-V279S/MPP complexes suggest valuable information to design future inhibitors for *Sco* GlgE-V279S and the homologous *Mtb* GlgE. With this assessment, it seems that endocyclic amines are preferable to α-exocyclic amines because the approach of the positively charged group toward the Glu 423 side chain does not encroach upon the volume of space occupied by the Asp 394 side chain and therefore would not promote protein structural changes that are detrimental to inhibitor binding. Additionally, while GlgE can accommodate the axial hydroxyl

moieties at positions 2 and 3, it seems that only the axial C(3)-OH group in **8** strongly supports binding. Specifically, the benefit of an axial C(3)-OH is that it interacts directly with the Asp 394 side chain affording a bidentate interaction between the inhibitor and the enzyme nucleophile. In contrast, the axial C(2)-OH in **8** does not form any notable interactions with the enzyme. Indeed, the presence of an equatorial C(2)-OH group is beneficial for binding since it forms two hydrogen bonded interactions with amino acid residues in the -1 subsite. Further, in the -1 subsite of all the compound bound structures of *Sco* GlgE1-V279S, we observe some volume that can be targeted with additional functional groups. Therefore, we can extend the length of the new inhibitors to access those unoccupied areas and form additional interactions with the conserved amino acid residues present in those areas.

Conclusions

The results obtained in these studies relate to both synthesis and structural evaluation of aminocarbocycles as inhibitors of GH13 enzymes. Herein, we have analyzed the diastereoselectivity of the Grignard reaction using the Cram's-chelate TS model. It is noted that the selectivity follows the rule for 4-α-glucoside series. However, there is an erosion of stereoselectivity in the 4-α-glucoside series (4:1) with respect to the gluco series (9:1). We were successful in identifying the desired isomer **27A** after subjecting the obtained dienes (**27A** and **27B**) to RCM and comparing their spectral data with the alkenes **17A** and **17B**. The success of the synthetic route was highly dependent on the development of suitable experimental conditions due to highly sensitive nature of the Grubb's RCM. Also, we have successfully synthesized and determined the stereochemistry of the target 1-aminocarbasugars **7** and **8**. In the case of **7**, the stereoselectivity of the hydrogenation was improved relative to the gluco series. Of these two compounds, **8** exhibited inhibitory activity of the enzyme at a modest IC_{50} value of 484 ± 51 μM. Compound **8** formed each of the expected interactions in the -2 subsite as these are consistent with previously published *Sco* GlgE1-V279S structures. The origins of the inhibitory ability of **8** derives from the flattened ring system, coulombic interactions with conserved active site residues, and the ability to adopt a E_2 conformation in the cyclohexene fragment. This causes the 3-OH to form a new hydrogen bond with the catalytic nucleophile while also maintaining an electrostatic interaction between the exocyclic amine and the general acid/general base Glu 423. We note an E_2 conformation of **8** bears similarity to either $^3S_1$, $^3H_4$ or even $B_{2,5}$ conformations that are possible for the conformational literary of natural substrates. However, this conformation could also be a result of the favorable Glu 423 - ammonium electrostatic interaction which would be absent in a $^2H_3$ conformation and the low interconversion barrier for $^2H_3$ to $^3H_2$. Overall, the inclusion of the exocyclic amine was not as beneficial to binding as expected. While the short polar interactions between the amine and Glu 423 are likely stabilizing complex formation, this benefit is negated in the complex with compound **7** due to unexpected protein structural changes induced by steric hindrance. In conclusion, we have reported an effective regiospecific method to prepare the 4-α-glucosides of 1-aminocarbasugars using a readily available starting material. This structural and inhibitory information provides valuable insights into the atomic

level understanding of valienamine-based GH inhibitor interactions and reveals new avenues for the design of improved inhibitors based on this important scaffold.

Declarations

Acknowledgements

Initial X-ray diffraction experiments were performed at The UNMC Structural Biology Core Facility which is funded by the Fred and Pamela Buffett NCI Cancer Center Support Grant (P30CA036727). X-ray diffraction datasets were ultimately obtained using resources of the Advanced Photon Source, a U.S. department of Energy (DOE) Office of Science User Facility operated for the DOE Office of Science by Argonne. National Laboratory under Contract No.DE-AC02-06CH11357. Use of the LS-CAT Sector 21 was supported by the Michigan Economics Development Corporation and Michigan Technology Tri-Corridor (Grant 085P1000817). NIH Grant R01AI105084 to D.R.R and S.J.S.

References

1. Davies, G. J., Gloster, T. M. & Henrissat, B. Recent structural insights into the expanding world of carbohydrate-active enzymes. *Current Opinion in Structural Biology.* **15**, 637–645 https://doi.org/10.1016/j.sbi.2005.10.008 (2005).
2. Rempel, B. P. & Withers, S. G. Covalent inhibitors of glycosidases and their applications in biochemistry and biology. *Glycobiology.* **18**, 570–586 https://doi.org/10.1093/glycob/cwn041 (2008).
3. Gloster, T. M. Development of inhibitors as research tools for carbohydrate-processing enzymes. *Biochem. Soc. Trans.* **40**, 913–928 https://doi.org/10.1042/Bst20120201 (2012).
4. Speciale, G., Thompson, A. J., Davies, G. J. & Williams, S. J. Dissecting conformational contributions to glycosidase catalysis and inhibition. *Current Opinion in Structural Biology.* **28**, 1–13 https://doi.org/10.1016/j.sbi.2014.06.003 (2014).
5. Sanchez-Fernandez, E. M., Fernandez, J. M. G. & Mellet, C. O. Glycomimetic-based pharmacological chaperones for lysosomal storage disorders: lessons from Gaucher, G(M1)-gangliosidosis and Fabry diseases. *Chem. Commun.* **52**, 5497–5515 https://doi.org/10.1039/c6cc01564f (2016).
6. Platt, F. M. Emptying the stores: lysosomal diseases and therapeutic strategies. *Nature Reviews Drug Discovery.* **17**, 133–150 https://doi.org/10.1038/nrd.2017.214 (2018).
7. Gloster, T. M. & Davies, G. J. Glycosidase inhibition: assessing mimicry of the transition state. *Org. Biomol. Chem.* **8**, 305–320 https://doi.org/10.1039/b915870g (2010).
8. Arjona, O., Gomez, A. M., Lopez, J. C. & Plumet, J. Synthesis and conformational and biological aspects of carbasugars. *Chemical reviews.* **107**, 1919–2036 (2007).
9. Lillelund, V. H., Jensen, H. H., Liang, X. & Bols, M. Recent developments of transition-state analogue glycosidase inhibitors of non-natural product origin. *Chemical reviews.* **102**, 515–554 (2002).

10. Colombo, C. & Bennet, A. J. Probing Transition State Analogy in Glycoside Hydrolase Catalysis. *Advances in Physical Organic Chemistry.* **Vol 51 51**, 99–127 https://doi.org/10.1016/bs.apoc.2017.09.001 (2017).
11. Olsen, K., Christensen, U., Sierks, M. R. & Svensson, B. Reaction mechanisms of Trp120–>Phe and wild-type glucoamylases from Aspergillus niger. Interactions with maltooligodextrins and acarbose. *Biochemistry.* **32**, 9686–9693 https://doi.org/10.1021/bi00088a021 (1993).
12. Mosi, R. *et al.* Reassessment of acarbose as a transition state analogue inhibitor of cyclodextrin glycosyltransferase. *Biochemistry.* **37**, 17192–17198 https://doi.org/10.1021/bi981109a (1998).
13. Shidmoossavee, F. S., Watson, J. N. & Bennet, A. J. Chemical Insight into the Emergence of Influenza Virus Strains That Are Resistant to Relenza. *Journal of the American Chemical Society.* **135**, 13254–13257 https://doi.org/10.1021/ja405916q (2013).
14. Tanaka, K. S., Winters, G. C., Batchelor, R. J., Einstein, F. W. & Bennet, A. J. A new structural motif for the design of potent glucosidase inhibitors. *Journal of the American Chemical Society.* **123**, 998–999 (2001).
15. Schmidt, D. D. *et al.* alpha-Glucosidase inhibitors. New complex oligosaccharides of microbial origin. *Naturwissenschaften.* **64**, 535–536 https://doi.org/10.1007/BF00483561 (1977).
16. Junge, B. *et al.* Studies on the Structure of the Alpha-D-Glucosidase Inhibitor Acarbose. *Carbohydr. Res.* **128**, 235–268 https://doi.org/10.1016/0008-6215(84)85333-1 (1984).
17. FURUMOTO, T., YOSHIOKA, T., KAMEDA, K. A. M. A. T. A. K., MATSUI, K. & Y. & Enzymic synthesis of valienamine glucosides and their antibiotic activity. *The Journal of antibiotics.* **44**, 371–373 (1991).
18. FURUMOTO, T., KAMEDA, Y. & MATSUI, K. Enzymatic synthesis of glucoside derivatives of validamine and valienamine. *Chemical and pharmaceutical bulletin.* **40**, 1871–1875 (1992).
19. Chen, X., Fan, Y., Zheng, Y. & Shen, Y. Properties and production of valienamine and its related analogues. *Chemical reviews.* **103**, 1955–1978 (2003).
20. Dabhi, A. S., Bhatt, N. R. & Shah, M. J. Voglibose: an alpha glucosidase inhibitor. *Journal of clinical and diagnostic research: JCDR.* **7**, 3023 (2013).
21. Goldsmith, E. J., Fletterick, R. J. & Withers, S. G. The three-dimensional structure of acarbose bound to glycogen phosphorylase. *J Biol Chem.* **262**, 1449–1455 (1987).
22. Qian, M. X., Haser, R., Buisson, G., Duee, E. & Payan, F. The Active-Center of a Mammalian Alpha-Amylase - Structure of the Complex of a Pancreatic Alpha-Amylase with a Carbohydrate Inhibitor Refined to 2.2-Angstrom Resolution. *Biochemistry.* **33**, 6284–6294 https://doi.org/10.1021/bi00186a031 (1994).
23. Abadi, S. S. K. *et al.* New Class of Glycoside Hydrolase Mechanism-Based Covalent Inhibitors: Glycosylation Transition State Conformations. *Journal of the American Chemical Society.* **139**, 10625–10628 https://doi.org/10.1021/jacs.7b05065 (2017).
24. Vocadlo, D. J. & Davies, G. J. Mechanistic insights into glycosidase chemistry. *Curr Opin Chem Biol.* **12**, 539–555 https://doi.org/10.1016/j.cbpa.2008.05.010 (2008).

25. Davies, G. J., Planas, A. & Rovira, C. Conformational Analyses of the Reaction Coordinate of Glycosidases. *Accounts of Chemical Research.* **45**, 308–316 https://doi.org/10.1021/ar2001765 (2012).
26. Kalscheuer, R. *et al.* Self-poisoning of Mycobacterium tuberculosis by targeting GlgE in an alpha-glucan pathway. *Nature Chemical Biology.* **6**, 376–384 https://doi.org/10.1038/nchembio.340 (2010).
27. Veleti, S. K., Lindenberger, J. J., Thanna, S., Ronning, D. R. & Sucheck, S. J. Synthesis of a poly-hydroxypyrolidine-based inhibitor of Mycobacterium tuberculosis GlgE. *The Journal of organic chemistry.* **79**, 9444–9450 (2014).
28. McCarter, J. D. & Withers, G. S. Mechanisms of enzymatic glycoside hydrolysis. *Current opinion in structural biology.* **4**, 885–892 (1994).
29. Koshland, D. Jr Stereochemistry and the mechanism of enzymatic reactions. *Biological reviews.* **28**, 416–436 (1953).
30. Woods, R. J., Andrews, C. W. & Bowen, J. P. Molecular mechanical investigations of the properties of oxocarbenium ions. 2. Application to glycoside hydrolysis. *Journal of the American Chemical Society.* **114**, 859–864 (1992).
31. Males, A., Speciale, G., Williams, S. J. & Davies, G. J. Distortion of mannoimidazole supports a B 2, 5 boat transition state for the family GH125 α-1, 6-mannosidase from Clostridium perfringens. *Organic & biomolecular chemistry.* **17**, 7863–7869 (2019).
32. Kameda, Y. & Horii, S. The unsaturated cyclitol part of the new antibiotics, the validamycins.*Journal of the Chemical Society, Chemical Communications*,746–747(1972).
33. KAMEDA, Y., Asano, N., Yoshikawa, M. & Matsui, K. Valienamine as an α-glucosidase inhibitor. *The Journal of Antibiotics.* **33**, 1575–1576 (1980).
34. Kapferer, P., Sarabia, F. & Vasella, A. Carbasaccharides via Ring-Closing Alkene Metathesis. A Synthesis of (+)-Valienamine from D-Glucose. *Helvetica chimica acta.* **82**, 645–656 (1999).
35. Chiara, J. L., Bobo, S. & Sesmillo, E. Stereoselective Synthesis of Branched Cyclopentitols by Titanium (III)-Promoted Reductive Cyclization of 4-Oxiranylaldehydes and 4-Oxiranyl Ketones Derived from Hexoses. (2008).
36. Pfitzner, K. & Moffatt, J. A new and selective oxidation of alcohols. *Journal of the American Chemical Society.* **85**, 3027–3028 (1963).
37. Chérest, M., Felkin, H. & Prudent, N. Torsional strain involving partial bonds. The stereochemistry of the lithium aluminium hydride reduction of some simple open-chain ketones. *Tetrahedron Lett.* **9**, 2199–2204 (1968).
38. Lim, C., Baek, D. J., Kim, D., Youn, S. W. & Kim, S. Efficient Synthesis of (+)-MK7607 and its C-1 Epimer via the Stereoselective Transposition of a Tertiary Allylic Alcohol. *Org. Lett.* **11**, 2583–2586 (2009).
39. Wong, S. S. & Paddon-Row, M. N. The importance of electrostatic effects in controlling π-facial stereoselectivity in nucleophilic additions to carbonyl compounds: an ab initio MO study of a

prototype chelation model.*Journal of the Chemical Society, Chemical Communications*,327–330(1991).

40. Ichikawa, Y. New synthetic method for allylic isocyanates through [3, 3] sigmatropic rearrangement of allylic cyanates. *Synlett.* **1991**, 238–240 (1991).
41. Fukase, H. & Horii, S. Synthesis of valiolamine and its N-substituted derivatives AO-128, validoxylamine G, and validamycin G via branched-chain inosose derivatives. *The Journal of Organic Chemistry.* **57**, 3651–3658 (1992).
42. Huang, L. C., Liang, P. H., Liu, C. Y. & Lin, C. C. Large-scale synthesis of per-O-acetylated saccharides and their sequential transformation to glycosyl bromides and thioglycosides. *Journal of carbohydrate chemistry.* **25**, 303–313 (2006).
43. Wessel, H. P., Mayer, B. & Englert, G. All-α-d-linked tetra-and penta-saccharide substructures of Trestatin A by block syntheses with triflic anhydride as promoter. *Carbohydrate research.* **242**, 141–151 (1993).
44. Motawia, M. S., Olsen, C. E., Møller, B. L. & Marcussen, J. Chemical synthesis and NMR spectra of a protected branched-tetrasaccharide thioglycoside, a useful intermediate for the synthesis of branched oligosaccharides. *Carbohydrate research.* **252**, 69–84 (1994).
45. Veleti, S. K., Lindenberger, J. J., Ronning, D. R. & Sucheck, S. J. Synthesis of a C-phosphonate mimic of maltose-1-phosphate and inhibition studies on Mycobacterium tuberculosis GlgE. *Bioorganic & medicinal chemistry.* **22**, 1404–1411 (2014).
46. Fleming, F. F., Wei, G. & Cyclohexanecarbonitriles Assigning Configurations at Quaternary Centers from 13C NMR CN Chemical Shifts. *The Journal of organic chemistry.* **74**, 3551–3553 (2009).
47. Kozikowski, A., Ognyanov, V., Chen, C., Kurian, P. & Crews, F. Synthesis and binding studies of an optically pure hexadeoxy-1, 4, 5-tris (methylenesulfonic acid) analogue of IP3. *Tetrahedron letters.* **34**, 219–222 (1993).
48. Chang, H. J., Zhu, J. R., Feng, X. L. & Xu, H. D. (+)-(1S, 2S, 3S, 4R, 5R)-1-Ammonio-5-hydroxymethylcyclohexane-2, 3, 4-triol chloride. *Acta Crystallographica Section E: Structure Reports Online.* **60**, o1712–o1714 (2004).
49. Yoshikawa, M. *et al.* Syntheses of validamine, epi-validamine, and valienamine, three optically active pseudo-amino-sugars, from D-glucose. *Chemical and pharmaceutical bulletin.* **36**, 4236–4239 (1988).
50. Syson, K. *et al.* Structure of Streptomyces maltosyltransferase GlgE, a homologue of a genetically validated anti-tuberculosis target. *Journal of Biological Chemistry.* **286**, 38298–38310 (2011).
51. Lindenberger, J. J., Veleti, S. K., Wilson, B. N., Sucheck, S. J. & Ronning, D. R. Crystal structures of Mycobacterium tuberculosis GlgE and complexes with non-covalent inhibitors. *Scientific reports.* **5**, 12830 (2015).
52. Veleti, S. K., Petit, C., Ronning, D. R. & Sucheck, S. J. Zwitterionic pyrrolidene-phosphonates: inhibitors of the glycoside hydrolase-like phosphorylase Streptomyces coelicolor GlgEI-V279S. *Organic & biomolecular chemistry.* **15**, 3884–3891 (2017).

53. Syson, K. *et al.* Structural insight into how Streptomyces coelicolor maltosyl transferase GlgE binds α-maltose 1-phosphate and forms a maltosyl-enzyme intermediate. *Biochemistry-Us.* **53**, 2494–2504 (2014).
54. Nielsen, J. E. & Borchert, T. V. Protein engineering of bacterial α-amylases. *Biochimica et Biophysica Acta (BBA)-Protein Structure and Molecular Enzymology.* **1543**, 253–274 (2000).
55. Mueller, M. & Nidetzky, B. The role of Asp-295 in the catalytic mechanism of Leuconostoc mesenteroides sucrose phosphorylase probed with site-directed mutagenesis. *FEBS letters.* **581**, 1403–1408 (2007).
56. Deslongchamps, P. Stereoelectronic effects in organic chemistry(Pergamon Press, 1983).
57. Uitdehaag, J. C. M. *et al.* X-ray structures along the reaction pathway of cyclodextrin glycosyltransferase elucidate catalysis in the alpha-amylase family. *Nature Structural Biology.* **6**, 432–436 https://doi.org/10.1038/8235 (1999).
58. Hosie, L. & Sinnott, M. L. Effects of Deuterium Substitution Alpha and Beta to the Reaction Center, O-18 Substitution in the Leaving Group, and Aglycone Acidity on Hydrolyses of Aryl Glucosides and Glucosyl Pyridinium Ions by Yeast Alpha-Glucosidase - a Probable Failure of the Antiperiplanar-Lone-Pair Hypothesis in Glycosidase Catalysis. *Biochem. J..* **226**, 437–446 https://doi.org/10.1042/bj2260437 (1985).
59. Nerinckx, W., Desmet, T. & Claeyssens, M. Itineraries of enzymatically and non-enzymatically catalyzed substitutions at O-glycopyranosidic bonds. *Arkivoc.* **13**, 90–116 (2006).
60. Adabala, P. J. P., Shamsi Kazem Abadi, S., Akintola, O., Bhosale, S. & Bennet, A. J. Conformationally controlled reactivity of carbasugars uncovers the choreography of glycoside hydrolase catalysis. *The Journal of organic chemistry.* **85**, 3336–3348 (2020).
61. Miyazaki, T. & Park, E. Y. Structure–function analysis of silkworm sucrose hydrolase uncovers the mechanism of substrate specificity in GH13 subfamily 17 exo-α-glucosidases. *Journal of Biological Chemistry.* **295**, 8784–8797 (2020).
62. Mok, S. C., Teh, A. H., Saito, J. A., Najimudin, N. & Alam, M. Crystal structure of a compact α-amylase from Geobacillus thermoleovorans. *Enzyme and microbial technology.* **53**, 46–54 (2013).
63. Larsbrink, J., Izumi, A., Hemsworth, G. R., Davies, G. J. & Brumer, H. Structural enzymology of Cellvibrio japonicus Agd31B protein reveals α-transglucosylase activity in glycoside hydrolase family 31. *Journal of Biological Chemistry.* **287**, 43288–43299 (2012).
64. Agirre, J. *et al.* The structure of the AliC GH13 α-amylase from Alicyclobacillus sp. reveals the accommodation of starch branching points in the α-amylase family. *Acta Crystallographica Section D: Structural Biology.* **75**, 1–7 (2019).
65. Braitsch, M. *et al.* Synthesis of fluorinated maltose derivatives for monitoring protein interaction by 19F NMR. *Beilstein journal of organic chemistry.* **8**, 448–455 (2012).
66. Joseph, A. A. *et al.* TMSOTf-Catalyzed silylation: streamlined regioselective one-pot protection and acetylation of carbohydrates. *European Journal of Organic Chemistry* 2012, 744 (2012).

67. Lu, S. R., Lai, Y. H., Chen, J. H., Liu, C. Y. & Mong, K. K. T. Dimethylformamide: an unusual glycosylation modulator. *Angew. Chem. Int. Ed.* **50**, 7315–7320 (2011).
68. Liebschner, D. *et al.* Macromolecular structure determination using X-rays, neutrons and electrons: recent developments in Phenix. *Acta Crystallographica Section D: Structural Biology.* **75**, 861–877 (2019).
69. Emsley, P. & Cowtan, K. Coot: model-building tools for molecular graphics. *Acta Crystallogr., Sect D: Biol. Crystallogr.* **60**, 2126–2132 (2004).

Tables

Due to technical limitations, table 1 to 4 is only available as a download in the Supplemental Files section.

Figures

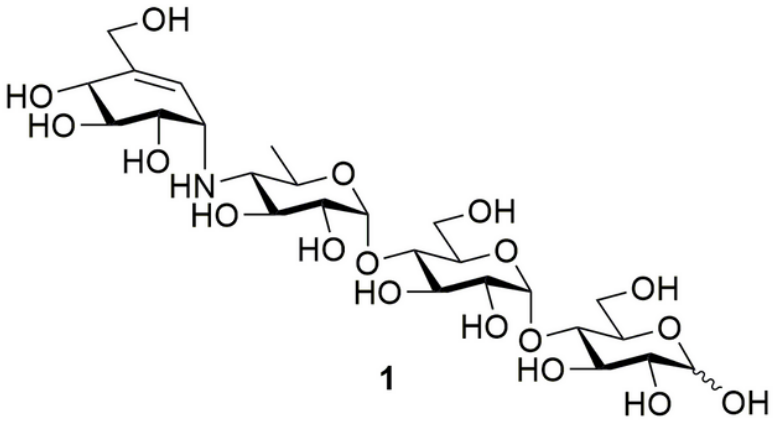

1

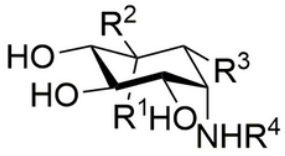

2a: R^1= H, R^2 = CH_2OH, R^3 = H, R^4 = H
2b: R^1= CH_2OH, R^2 = H, R^3 = H, R^4 = H

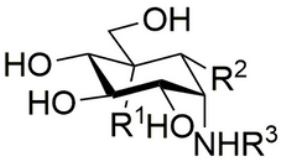

3: R^1= H, R^2 = OH, R^3 = H
4: R^1= OH, R^2 = H, R^3 = H
5: R^1= H, R^2 = H, R^3 = $CH(CH_2OH)_2$

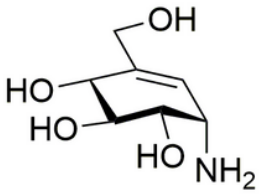

6

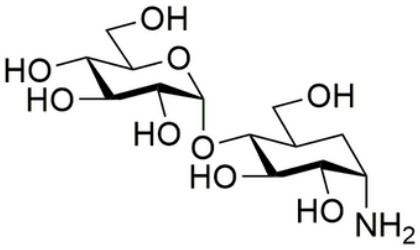

7

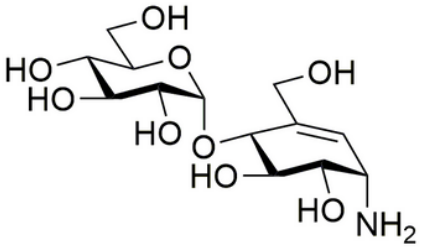

8

Figure 1

Aminocarbasugar-based GH inhibitors and targets 7 and 8.

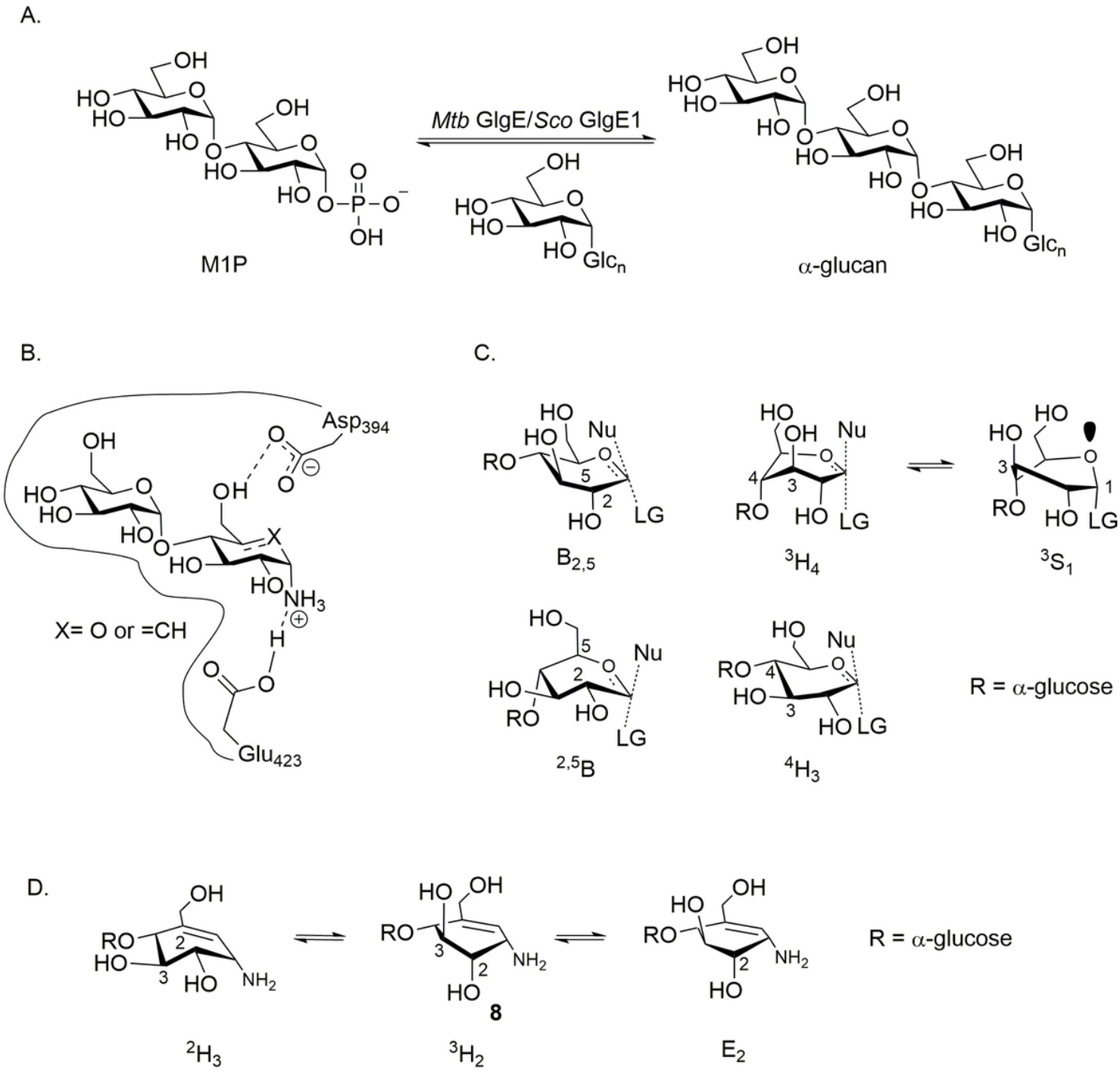

Figure 2

(A) Mtb GlgE/Sco GlgE1 catalyzed glycosylation of α-1,4 glucan with M1P. (B) Proposed Sco GlgE1-V279S/7 and Sco GlgE1-V279S/8 complex coulombic interactions. (C) B2,5, 2,5B, 4H3, and 3H4 C5–O5–C1–C2 planar TS conformations commonly invoked for GH and an 3S1 ALPH-compliant conformation shown in equilibrium with a 3H4 TS. (D) Possible conformations of the cyclohexene fragment of 8.

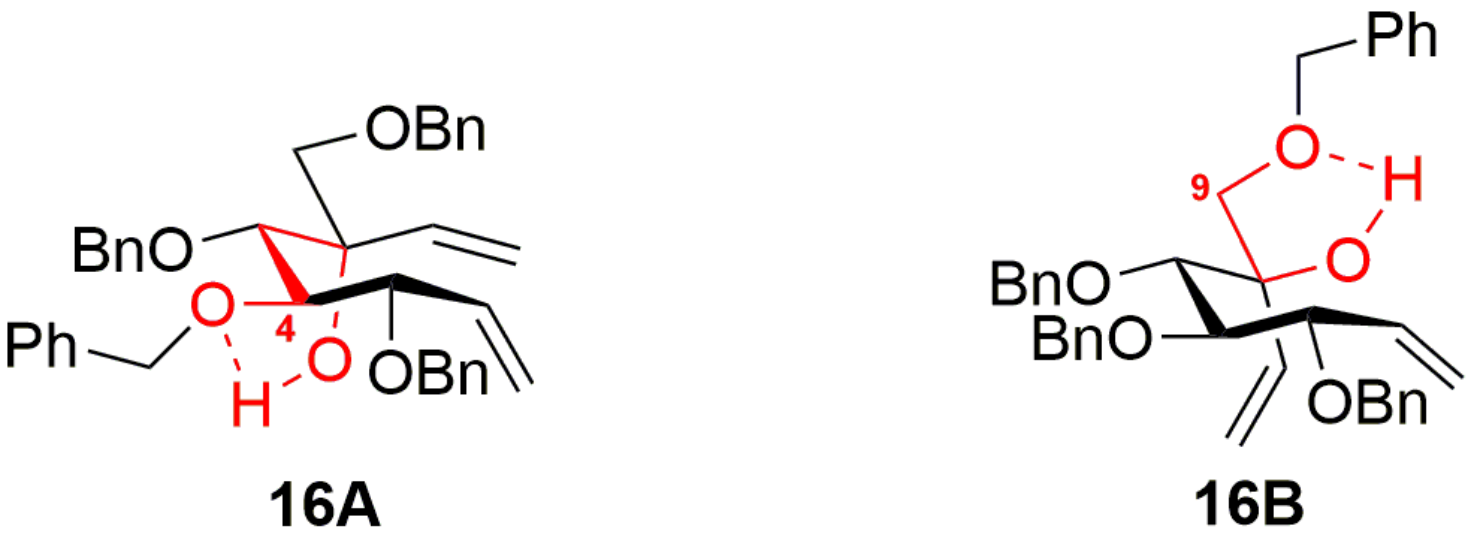

Figure 3

Intramolecular H-bonding interactions of the diastereomers 16A, 27A, 16B and 27B.

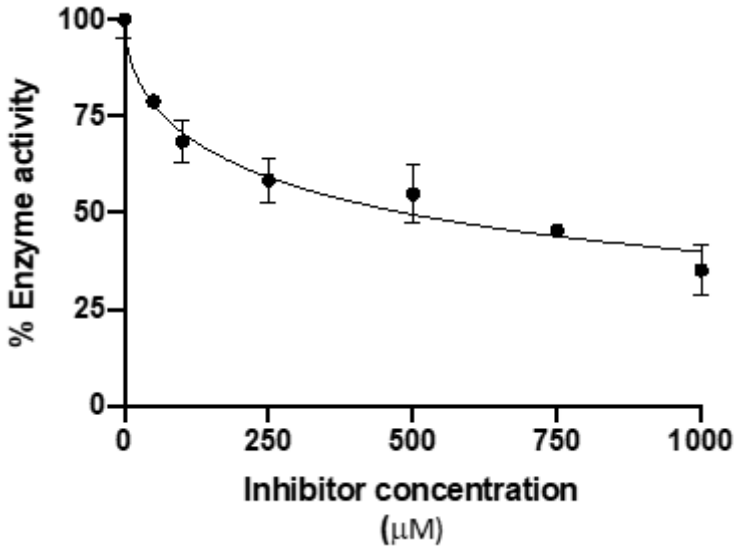

Figure 4

IC50 determination of 8 against Sco GlgE1-V279S. The error bars were calculated by using the results of triplicate reactions.

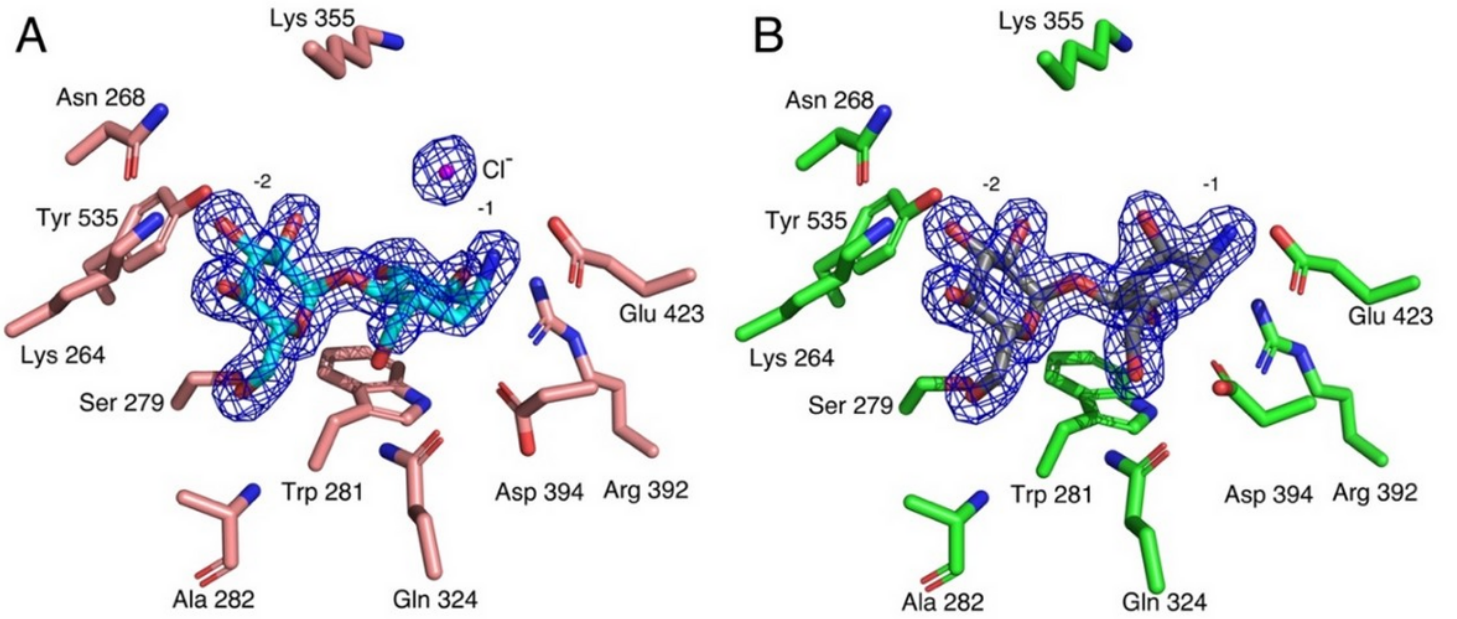

Figure 5

Compounds 7 and 8 bound in the active site of Sco GlgE1-V279S. (A) Complex of Sco GlgE1-V279S with 7. The magenta sphere represents the ordered chloride ion. (B) Complex of Sco GlgE1-V279S with 8. Both 2FO-FC composite omit maps are contoured at 1.5Ⓧ.

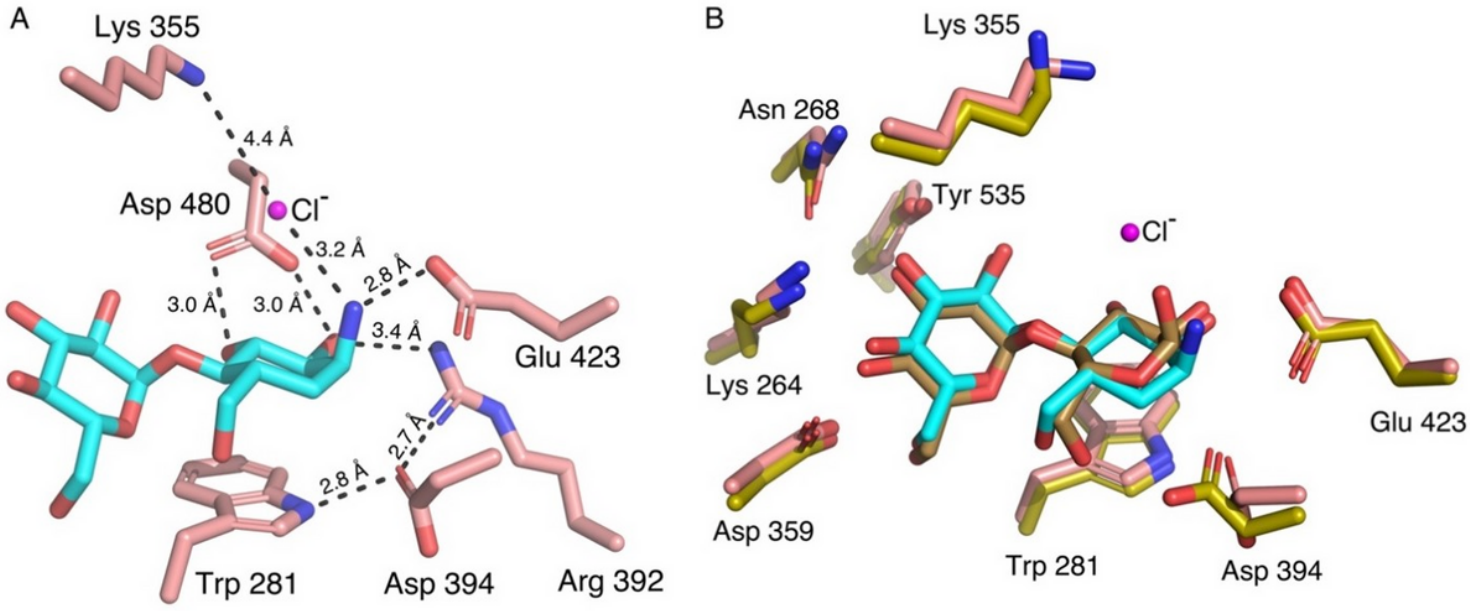

Figure 6

(A) The interactions formed in -1 subsite of Sco GlgE1-V279S with 7. (B) Superimposed active sites of Sco GlgE1-V279S/7 and Sco GlgE1/Maltose structures (yellow carbon atoms).

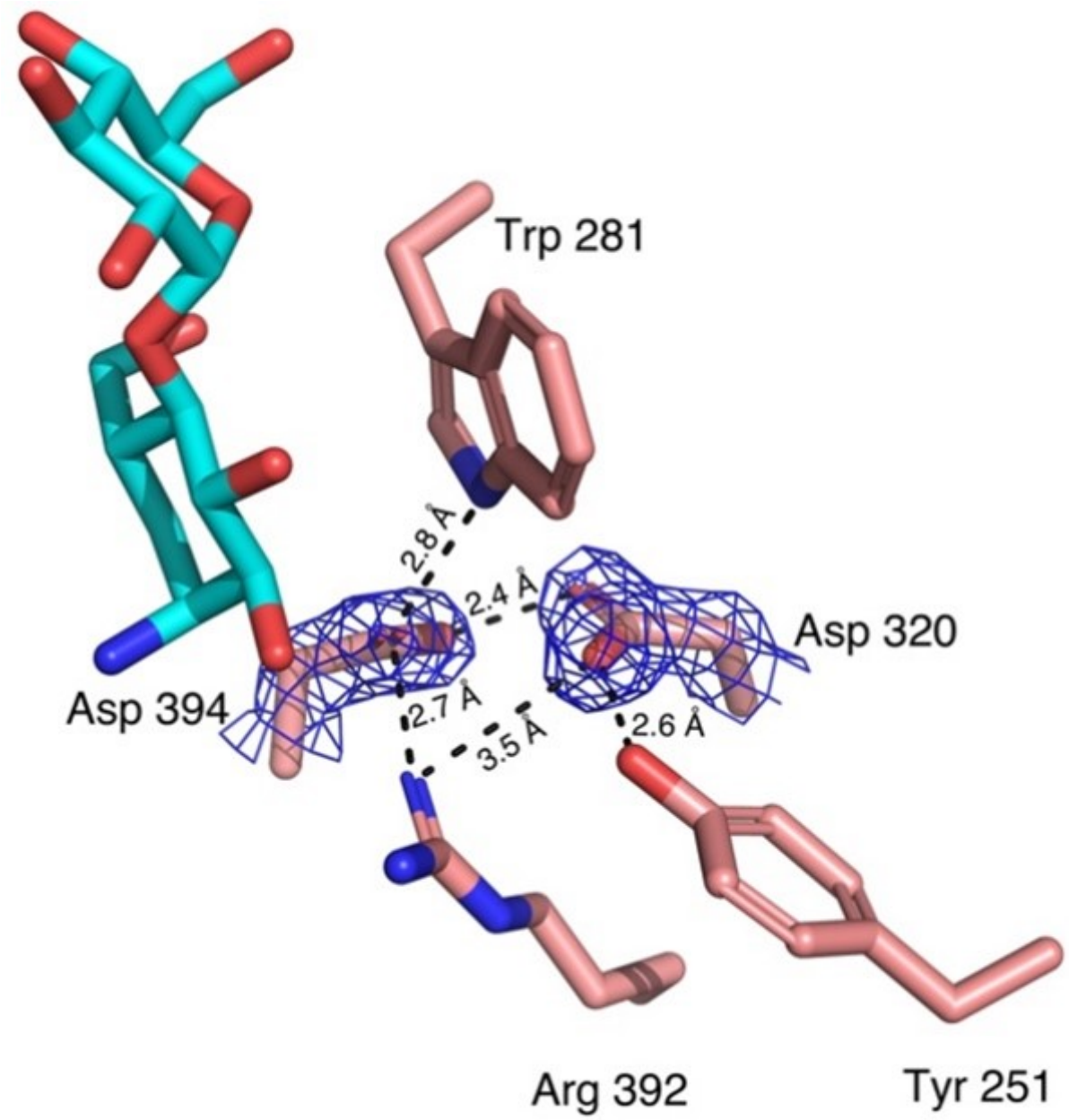

Figure 7

Interactions formed by shifted Asp 394 in Sco GlgE1-V279S/7, the composite 2FO-FC omit map was contoured at 1.5.

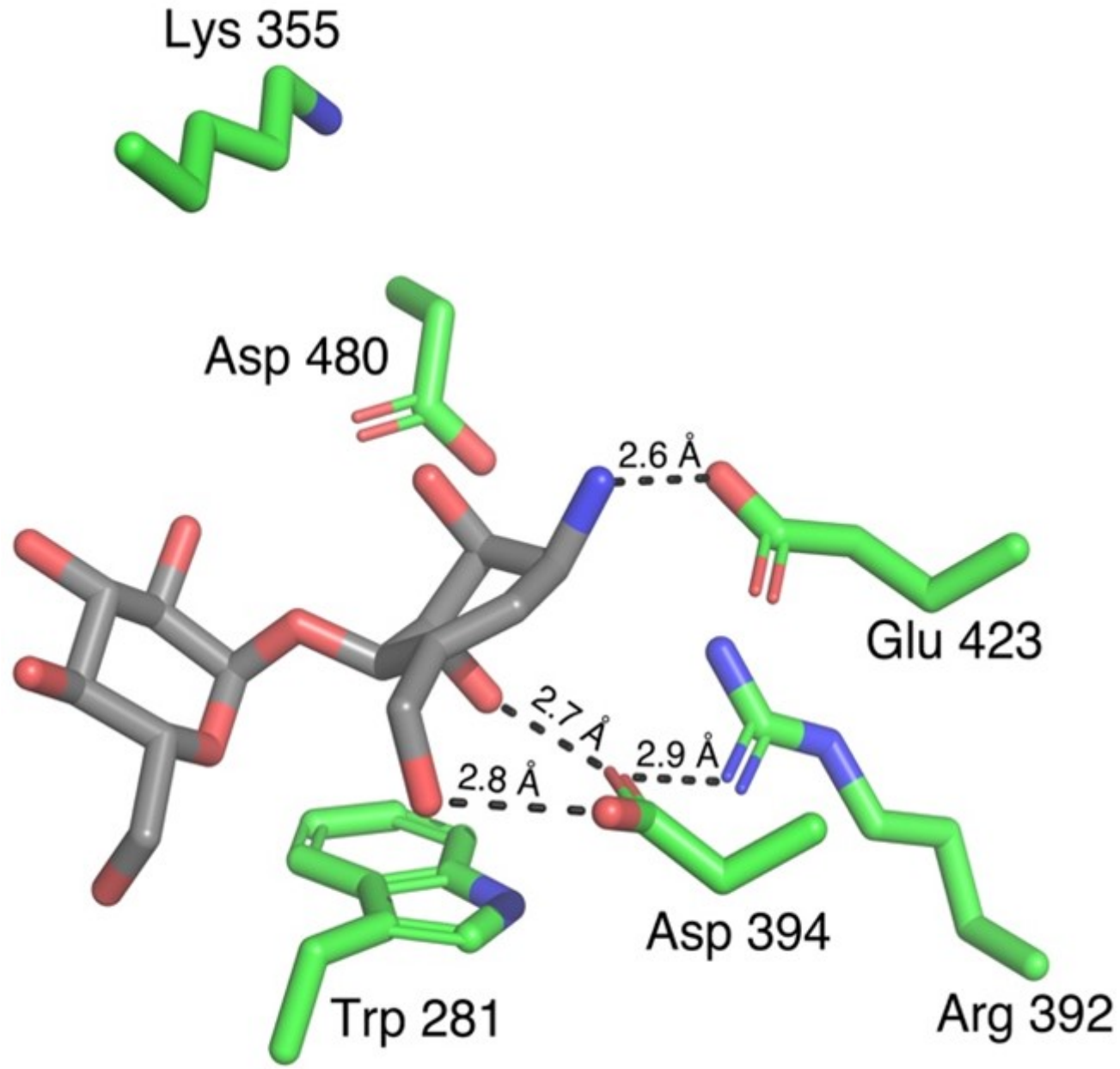

Figure 8

The interactions formed in the -1 subsite of Sco GlgE1-V279S with 8.

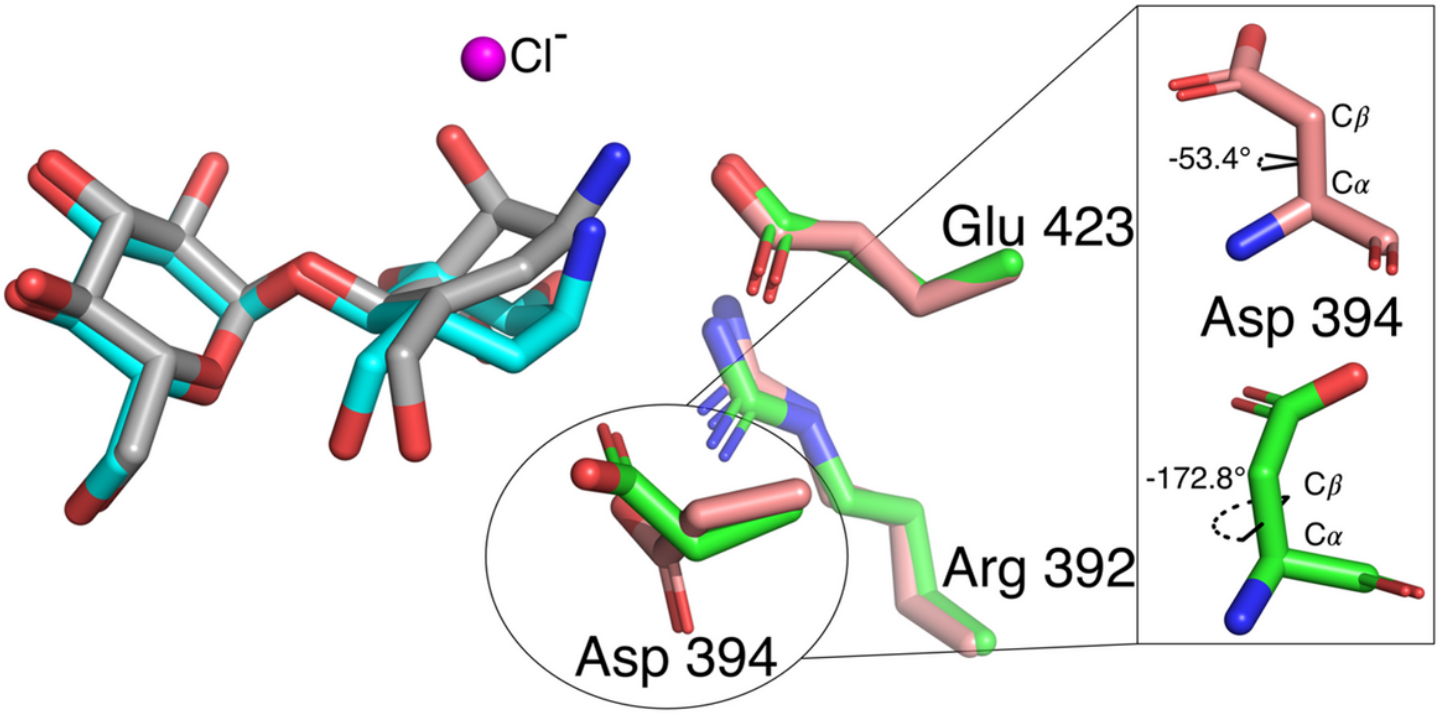

Figure 9

Superimposed active sites of Sco GlgE1-V279S/7 and Sco GlgE1-V279S/8 structures.

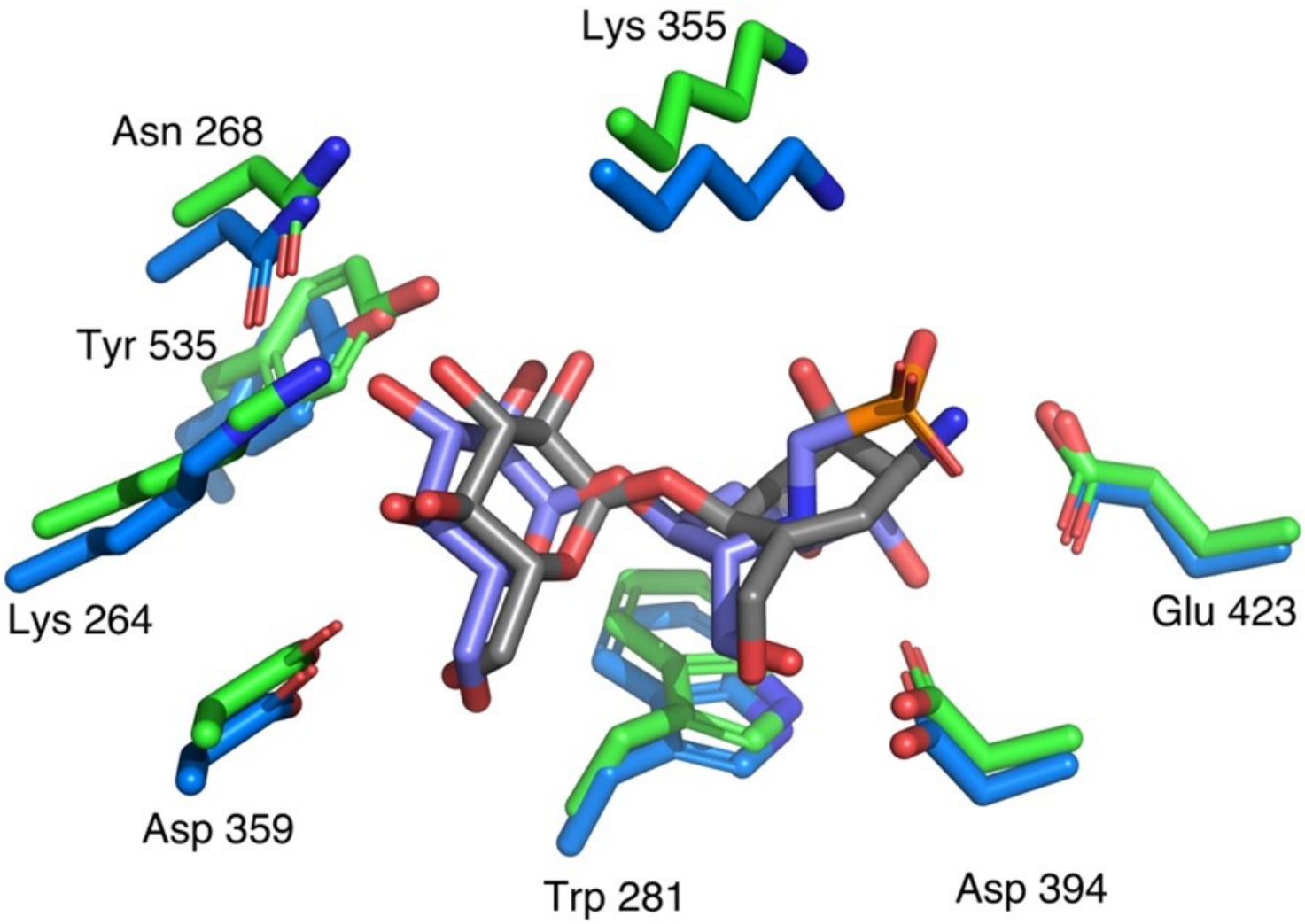

Figure 10

Superimposed active sites of Sco GlgE1-V279S/8 and Sco GlgE1-V279S/MPP structures.

Supplementary Files

This is a list of supplementary files associated with this preprint. Click to download.

- Table1.tif
- Table2.tif
- Table3.tif
- Table4.tif
- Scheme1.png
- Scheme2.png
- Scheme3.png
- Scheme4.png

- Scheme5.png
- supportinginfoaminosugarsfinal.docx